Published in final edited form as:

Cell Rep. 2024 September 24; 43(9): 114674. doi:10.1016/j.celrep.2024.114674.

Lysosome-related organelle integrity suppresses TIR-1 aggregation to restrain toxic propagation of p38 innate immunity

Samantha Y. Tse-Kang[1], **Read Pukkila-Worley**[1,2,*]

[1]Program in Innate Immunity, Division of Infectious Diseases and Immunology, Department of Medicine, UMass Chan Medical School, Worcester, MA, USA

[2]Lead contact

SUMMARY

Innate immunity in bacteria, plants, and animals requires the specialized subset of Toll/interleukin-1/resistance gene (TIR) domain proteins that are nicotinamide adenine dinucleotide (NAD^+) hydrolases. Aggregation of these TIR proteins engages their enzymatic activity, but it is unknown how this protein multimerization is regulated. Here, we discover that TIR oligomerization is controlled to prevent immune toxicity. We find that p38 propagates its own activation in a positive feedback loop, which promotes the aggregation of the lone enzymatic TIR protein in the nematode *C. elegans* (TIR-1, homologous to human sterile alpha and TIR motif-containing 1 [SARM1]). We perform a forward genetic screen to determine how the p38 positive feedback loop is regulated. We discover that the integrity of the specific lysosomal subcompartment that expresses TIR-1 is actively maintained to limit inappropriate TIR-1 aggregation on the membranes of these organelles, which restrains toxic propagation of p38 innate immunity. Thus, innate immunity in *C. elegans* intestinal epithelial cells is regulated by specific control of TIR-1 multimerization.

Graphical Abstract

*Correspondence: read.pukkila-worley@umassmed.edu.

AUTHOR CONTRIBUTIONS

Conceptualization, S.Y.T.-K. and R.P.-W.; methodology, S.Y.T.-K. and R.P.-W.; investigation, S.Y.T.-K.; visualization, S.Y.T.-K.; funding acquisition, R.P.-W.; project administration, R.P.-W.; supervision, R.P.-W.; writing – original draft, S.Y.T.-K. and R.P.-W.; writing – review & editing, S.Y.T.-K. and R.P.-W.

DECLARATION OF INTERESTS

The authors declare no competing interests.

SUPPLEMENTAL INFORMATION

Supplemental information can be found online at https://doi.org/10.1016/j.celrep.2024.114674.

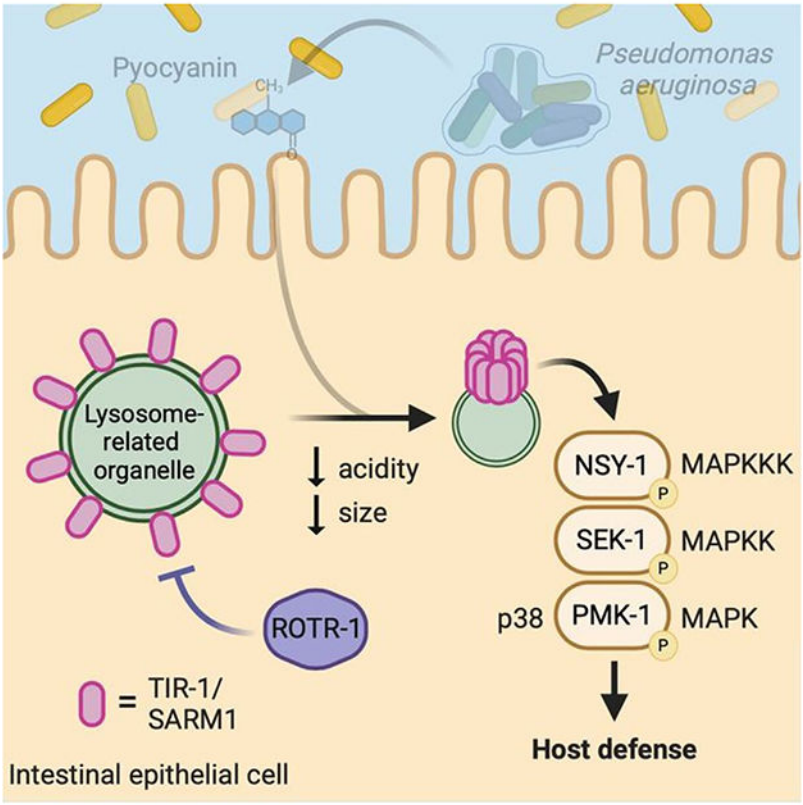

In brief

Innate immunity across the tree of life requires enzymatic TIR-domain proteins, whose activity is engaged by aggregation. However, it is not known how this protein multimerization is regulated. Tse-Kang et al. discovered that the integrity of lysosome-related organelles, which express TIR-1, is actively maintained in *C. elegans* to limit inappropriate TIR-1 aggregation and toxic propagation of innate immunity.

INTRODUCTION

Tight control of inflammation is essential for animal health and is a particular challenge for cells in barrier tissues, such as the intestinal epithelium, that constantly interface with both commensal organisms and virulent pathogens. Conceptually, pathogen-sensing mechanisms, which activate protective inflammatory signaling cascades during infection, must themselves be regulated to prevent pathology associated with exuberant immune activation. How this occurs, however, is not fully understood.

In this study, we define an immunoregulatory axis anchored by a protein whose function in innate immunity is conserved across the Tree of Life. A specific subset of proteins that contain Toll/interleukin-1/resistance gene (TIR) domains are enzymes that metabolize nicotinamide adenine dinucleotide (NAD^+) to produce secondary metabolites.[1-3] Like other proteins with a TIR domain, which include Toll-like receptors in animals, these proteins are essential for coordinating host defense against pathogen infection. The catalytic activity of

plant TIR, for example, is required to induce protective cell death responses during pathogen infection.[2] Enzymatic TIR proteins also function in bacterial immunity, orchestrating protective anti-phage defenses.[4] It is noteworthy that the enzymatic activity of TIR is often dependent on protein oligomerization. For example, plant TIR forms a tetrameric structure upon activation that drives its catalytic activity.[5,6] In addition, prokaryotic TIR-containing proteins oligomerize into filaments to induce NAD^+ hydrolase activity.[3] A TIR-containing protein with enzymatic activity in animals and humans, sterile alpha and TIR motif-containing 1 (SARM1), requires multimerization to engage its intrinsic NAD^+ hydrolase activity.[7,8] Oligomerization of enzymatic TIR proteins is therefore conserved across millions of years of evolution; however, it is not known how TIR multimerization is regulated.

TIR-1 in the nematode *C. elegans* is the homolog of mammalian SARM1. TIR-1 functions upstream of the p38 PMK-1 mitogen-activated protein kinase (MAPK) and is required for host defense against infection with a variety of pathogens.[9-11] Previously, we discovered that TIR-1 multimerizes in intestinal epithelial cells during pathogen infection.[12] Oligomerization of TIR-1 in this manner engages its intrinsic NAD^+ hydrolase activity[8,12,13] to activate the p38 PMK-1 pathway.[12] In a companion manuscript co-submitted with this study, we discovered that TIR-1 is expressed on the membranes of lysosome-related organelles.[14] We found that pyocyanin, a virulence effector secreted by the bacterial pathogen *Pseudomonas aeruginosa*, alkalinized and condensed lysosome-related organelles. This morphological change in lysosome-related organelles triggered TIR-1 multimerization, which activated the p38 PMK-1 immune pathway to protect the host against microbial intoxication. Thus, TIR-1 is a guard protein in an effector-triggered immune response that allows *C. elegans* to sense the effects of pathogen infection on the host and activate innate immune defenses.

Here, we discovered that aberrant TIR-1 aggregation and activation in the intestine are toxic and, therefore, tightly controlled. Inappropriate activation of p38 PMK-1 is a well-known contributor to pathology. We show that these immune toxicities are regulated at the level of TIR-1. Our studies revealed that lysosome-related organelle integrity is actively maintained to suppress TIR-1 multimerization and restrain toxic p38 PMK-1 activation in *C. elegans*. We found that p38 PMK-1 drove a positive feedback loop, which potentiated its own activation by promoting the expression, aggregation, and activation of TIR-1. We performed a forward genetic screen to determine how positive feedback activation of p38 PMK-1 is controlled and identified a previously uncharacterized gene, which we named regulator of *tir-1* (*rotr-1*). ROTR-1 maintained the size of lysosome-related organelles, which promoted immune homeostasis by limiting aggregation and activation of TIR-1. Thus, our unbiased forward genetic screen identified *C. elegans* mutants that recapitulated the pathogen-induced damage to the specific lysosomal compartment that expresses TIR-1, providing orthologous confirmation for the cell biological characterization of p38 PMK-1 immune activation in our companion manuscript.[14] In addition, these data demonstrate that a lysosomal-TIR-1-p38 axis restrains immune activation in intestinal epithelial cells to promote healthy growth and longevity of *C. elegans*.

RESULTS

Positive feedback activation of the p38 PMK-1 pathway potentiates innate immune defenses by promoting TIR-1 multimerization

C. elegans TIR-1 activates the p38 PMK-1 immune pathway, a classic MAPK signaling cassette with the MAPKKK NSY-1 (homolog of mammalian ASK1), the MAPKK SEK-1 (homolog of mammalian MKK3/6), and p38 PMK-1. The phosphatase *vhp-1* dephosphorylates p38 PMK-1 to negatively regulate innate immune defenses (Figure S1A).[15] We examined the mechanisms of TIR-1 regulation and made the surprising observation that RNAi-mediated knockdown of *vhp-1*, which hyperactivates p38 PMK-1,[15] caused robust induction of TIR-1 protein expression (Figures 1A, 1B, and S1B). This result was unexpected because p38 PMK-1 is downstream of TIR-1 in the activation of innate immune defenses (Figure S1A).[9] For these studies, we used a *C. elegans* strain, previously engineered in our laboratory using clustered regularly interspaced short palindromic repeats (CRISPR)-Cas9, that expresses TIR-1 protein tagged at its endogenous locus with a 3xFLAG sequence (TIR-1::3xFLAG).[12] These data suggest that p38 PMK-1 may potentiate its own activation in a positive feedback cycle to propagate activation of anti-pathogen defenses.

Activation of p38 PMK-1 requires multimerization of TIR-1 into protein assemblies (puncta) in intestinal epithelial cells, which engages its intrinsic NAD^+ hydrolase activity.[12] We therefore explored whether *vhp-1(RNAi)* promoted TIR-1 aggregation. First, we examined TIR-1::3xFLAG under non-denaturing, or native, conditions. RNAi of *vhp-1* increased TIR-1 protein expression and induced the formation of higher-order multimers (Figures 1C and S1B). Second, we used a *C. elegans* strain that we previously engineered using CRISPR-Cas9, which expresses TIR-1 protein tagged with the fluorophore wrmScarlet at its endogenous genomic locus.[12] RNAi-mediated knockdown of *vhp-1* increased TIR-1::wrmScarlet protein expression and significantly induced the formation of TIR-1::wrmScarlet puncta in the intestine (Figures 1D and 1E). Thus, hyperactivation of the p38 PMK-1 pathway by *vhp-1(RNAi)* phenocopied the TIR-1 aggregation previously observed during pathogen infection.[12]

To test the hypothesis that p38 PMK-1 potentiates innate immune activation by increasing TIR-1 expression, we crossed the p38/*pmk-1(km25)* null mutant into the strain expressing TIR-1::3xFLAG. The p38/*pmk-1(km25)* mutation suppressed induction of TIR-1::3xFLAG protein by *vhp-1(RNAi)* (Figures 1A, 1B, and S1B). Some variability in TIR-1::3XFLAG induction was noted in this experiment, which we attributed to the efficiency of RNAi-mediated knockdown of *vhp-1* in these biological replicate experiments. The phosphatase *vhp-1* also dephosphorylates the MAP kinase *kgb-1*.[16] However, the *kgb-1(km21)* null allele did not suppress the induction of TIR-1::3xFLAG protein by *vhp-1(RNAi)*, demonstrating that the p38 PMK-1 pathway specifically induced TIR-1 in a positive feedback cycle (Figure S1C).

Consistent with the TIR-1 protein expression data, we also observed that knockdown of *vhp-1* induced the transcription of *tir-1* mRNA (Figure 1F). Importantly, the increased *tir-1* transcription observed in *vhp-1(RNAi)* animals was significantly suppressed in the

p38/pmk-1(km25) mutant background (Figure 1F). Thus, activation of *tir-1* transcription by the p38 PMK-1 pathway potentiated innate immune signaling by inducing TIR-1 multimerization. We propose that positive feedback propagation of immune defenses in this manner facilitates a rapid and robust response to challenge by an infectious pathogen.

A forward genetic screen identifies *rotr-1*, a suppressor of immune gene transcription

Constitutive activation of the p38 PMK-1 immune pathway is detrimental to the overall health of *C. elegans*.[17-21] Thus, we reasoned that positive feedback activation of p38 PMK-1 immune signaling is regulated to prevent the deleterious effects of unchecked innate immune activation. We performed a forward genetic screen to identify the mechanism that promotes this immune homeostasis. For these studies, we used a transcriptional reporter for the innate immune gene *irg-5 (irg-5p::gfp)* to provide a visual readout of p38 PMK-1 pathway activation. The gene *irg-5* encodes a secreted innate immune effector whose transcription is strongly induced in intestinal epithelial cells during infection with several different bacterial pathogens, including *P. aeruginosa*.[10,12,22,23] The basal expression of *irg-5* (i.e., in the absence of pathogen infection) depends on the p38 PMK-1 pathway,[10,24] and knockdown of *irg-5* alone renders *C. elegans* hypersusceptible to pathogen infection.[24] We therefore hypothesized that a genetic screen for mutants, which cause constitutive activation of *irg-5*, would uncover mechanisms that promote immune homeostasis in the *C. elegans* intestine.

Of 33,000 haploid mutant genomes screened from the F2 generation, nine mutant strains were recovered that hyperactivated *irg-5*p::*gfp* (Figure S2A). Three of these nine strains contained a mutation in Y42G9A.1 (*ums33, ums38, ums39*), a previously uncharacterized gene that we named *rotr-1* (Figure 2A). Both *ums33* and *ums39* had a missense mutation converting serine to phenylalanine at position 92 (S92F), and *ums38* carried a nonsense mutation at position 186 (N186*) (Figure 2A). We used RT-qPCR to confirm that the native *irg-5* gene was hyperactivated in *rotr-1(ums33), rotr-1(ums38)*, and *rotr-1(ums39)* loss-of-function mutants (Figure 2B). RNAi-mediated knockdown of *rotr-1* hyperactivated *irg-5*p::*gfp* (Figure 2C). Using CRISPR-Cas9, we generated a clean deletion mutant of *rotr-1* that spanned 4,621 bp of the *rotr-1* gene and 34 bp of the upstream promoter region *(rotr-1(ums53)). C. elegans rotr-1(ums53)* mutants recapitulated the hyperactivation of *irg-5*p::*gfp* observed in the *rotr-1* mutants recovered in the forward genetic screen (Figure 2D). We raised an antibody to the ROTR-1 protein and confirmed that this protein was not expressed in *rotr-1(ums53)* mutants, demonstrating that this is a null allele (Figure S2B). Reintroduction of *rotr-1* expressed under the control of its own promoter into *rotr-1(ums38)*, a mutant recovered in the forward genetic screen, suppressed the induction of *irg-5*p::*gfp* (Figure 2E).

mRNA sequencing (seq) revealed that putative immune effectors were strongly upregulated in *rotr-1(ums53)* mutants (Figure 2F). We compared the genes that were differentially regulated in *rotr-1(ums53)* mutants with genes whose expression was changed in wild-type *C. elegans* during infection with *P. aeruginosa*. These datasets significantly correlated with each other ($r = 0.778$, $p < 0.01$, black circles in Figure 2F). Intriguingly, the host defense genes that were differentially expressed in *rotr-1(ums53)* mutants were enriched in the upper right quadrant (red circles in Figure 2F), demonstrating that *rotr-1* suppressed the

expression of putative immune effectors. Of note, *irg-5*, the transcriptional reporter used in the forward genetic screen, was the most significantly upregulated gene in *rotr-1(ums53)* mutants, with a $\log_2$ fold change of 5.4 compared to wild-type animals (Figures 2F; Table S1). These data confirm that the recovery of *rotr-1* from the forward genetic screen was not secondary to pleiotropic effects of the mutant on transgene de-silencing. We confirmed the mRNA-seq data using RT-qPCR to assay the expression of three innate immune effectors in the *rotr-1(ums53)* clean deletion mutant: *irg-4* (Figure 2G), *irg-5* (Figure 2H), and T24B8.5 (*sysm-1*), a putative ShK-like protein dependent on p38 PMK-1 (Figure 2I).

In summary, a forward genetic screen identified *rotr-1*, a previously uncharacterized suppressor of immune gene transcription.

ROTR-1 suppresses positive feedback activation of p38 PMK-1 innate immunity

Gene set enrichment analysis of the RNA-seq data revealed that p38 PMK-1 targets were significantly enriched among the upregulated genes in *rotr-1(ums53)* (Figure 3A). Accordingly, *rotr-1(ums53)* activated a GFP transcriptional reporter for T24B8.5 (T24B8.5p::*gfp*) (Figure 3B).[10,11] To confirm that *rotr-1(ums53)* null mutants hyperactivated p38 PMK-1, we performed immunoblotting to quantify phosphorylated p38 PMK-1 compared to total p38 PMK-1. *C. elegans rotr-1(ums53)* null mutants had significantly higher levels of active p38 PMK-1 relative to wild-type animals (Figures 3C and 3D), consistent with the gene expression signature of these mutants. Importantly, the hyperphosphorylation of p38 PMK-1 in the *rotr-1(ums53)* mutants was suppressed in both the *tir-1(qd4)* and *pmk-1(km25)* loss-of-function backgrounds (Figures 3C and 3D). Consistent with these data, hyperactivation of the p38-dependent innate immune genes *irg-4* (Figure S3A), *irg-5* (Figure S3B), and T24B8.5 (Figure S3C) in the *rotr-1(ums53)* null mutants was suppressed in the absence of *tir-1* or *pmk-1*. Thus, ROTR-1 suppressed p38 PMK-1 pathway activation.

C. elegans rotr-1(ums53) mutants had significantly more TIR-1::wrmScarlet puncta than wild-type animals (Figures 3E and 3F). To determine whether TIR-1 protein levels were also increased in *rotr-1* mutants, we assessed TIR-1::3xFLAG protein expression by immunoblot. TIR-1::3xFLAG protein levels were significantly higher in *rotr-1(ums53)* mutants compared to wild-type animals (Figures 3G and 3H). In addition, *rotr-1(ums53)* null mutants had increased levels of higher-order multimers of TIR-1 compared to wild-type animals when examined under native conditions (Figures 3I and S3D). Thus, our data demonstrated that ROTR-1 acts upstream of TIR-1 to suppress p38 PMK-1 pathway activation.

Importantly, the increase in TIR-1 protein in *rotr-1(ums53)* mutants was suppressed by RNAi-mediated knockdown of p38 *pmk-1* (Figures 3G and 3H), which recapitulated our previous observations with *vhp-1(RNAi)* (Figure 1). In addition, *rotr-1(ums53)* mutants expressed significantly higher levels of *tir-1* mRNA compared to wild-type animals (Figure 3J). Thus, ROTR-1 suppressed the positive feedback activation of p38 PMK-1.

We generated a *gfp*-based transcriptional immune reporter for *rotr-1* to study its regulation. Knockdown of *vhp-1*, the phosphatase that negatively regulates p38 PMK-1, activated *rotr-1p::gfp* transcription (Figure 3K). In contrast, *tir-1*(RNAi) suppressed *rotr-1p::gfp*

transcription (Figure 3K). Using CRISPR-Cas9, we introduced a 3xFLAG tag at the endogenous N terminus of ROTR-1. As we observed in studies of *rotr-1p::gfp* transcription, *vhp-1(RNAi)* increased, and *tir-1(RNAi)* suppressed, 3xFLAG::ROTR-1 protein expression (Figure 3L). Thus, p38 PMK-1 pathway activation increased the expression of ROTR-1, a negative regulator of immune pathway signaling.

High-throughput interactome mapping of *C. elegans* proteins using yeast two-hybrid experiments previously found that ROTR-1 binds to TIR-1 *in vitro*.[26] These data raise the intriguing hypothesis that ROTR-1 physically restrains TIR-1 to suppress p38 PMK-1 activation. We therefore sought to determine if this protein-protein interaction occurs *in vivo*. Using CRISPR-Cas9, we introduced a 3xHA tag at the C terminus of ROTR-1 in an animal expressing TIR-1::3xFLAG. Unexpectedly, addition of the endogenous ROTR-1::3xHA tag induced TIR-1::3xFLAG protein expression (Figure S3E), phenocopying the upregulation of TIR-1 protein expression in *rotr-1(ums53)* null mutants (Figures 3G and 3H). To test whether this result was terminus specific, we used CRISPR-Cas9 to create two different strains that carried either a 3xFLAG or 3xHA tag at the N terminus of ROTR-1. However, the addition of these tags to ROTR-1 caused hyperactivation of the T24B8.5p::*gfp* reporter, which also phenocopied the *rotr-1(ums53)* mutation (Figures S3F and S3G). We conclude that tagging ROTR-1 at either the N or C termini disrupted the function of this protein, which precluded the ability to interpret data from co-immunoprecipitation experiments. Our attempts to use the antibody we raised against ROTR (Figure S2B) in co-immunoprecipitation experiments with TIR-1::3xFLAG were also unsuccessful secondary to non-specific protein binding by the ROTR-1 antibody. Nevertheless, these data provided additional confirmation of the phenotypes in the *rotr-1* loss-of-function mutant strain. In summary, ROTR-1 suppressed TIR-1 aggregation to restrain the positive feedback propagation of p38 PMK-1 immune signaling.

ROTR-1 supports the integrity of lysosome-related organelles, which suppresses positive feedback activation of p38 PMK-1 innate immunity.

In a companion manuscript, we discovered that the conserved signaling regulator TIR-1, the upstream activator of the p38 PMK-1 signaling cassette, is expressed on the membranes of a specific population of lysosomes called lysosome-related organelles.[14] Aggregation of TIR-1 into puncta following the pathogen-induced condensation of lysosome-related organelles engages the intrinsic NAD^+ hydrolase activity of this protein complex to activate p38 PMK-1 innate immune defenses.

In the mRNA-seq experiment (Figure 2), we also found that *rotr-1* regulated a significant number of genes involved in lysosomal function, including acid phosphatases and genes required for proteolysis (Figures S4A and S4B; Table S1). In light of the findings presented in our companion manuscript,[14] we hypothesized that ROTR-1 promotes the integrity of lysosome-related organelles, which in turn restrains positive feedback activation of p38 PMK-1 innate immunity. To test whether *rotr-1(ums53)* null mutants had defects in the lysosomal compartment, we used LysoTracker red, a dye that stains acidic organelles.[27,28] Compared to wild-type animals, *rotr-1(ums53)* mutants had significantly fewer vesicles that stained positively for LysoTracker red, demonstrating that the acidified cellular compartment

is compromised in this mutant background (Figures 4A and 4B). Importantly, in our companion manuscript, we discovered that both *P. aeruginosa* infection and treatment with the secreted pseudomonal virulence effector pyocyanin depleted LysoTracker red staining of acidic vesicles in intestinal epithelial cells.[14] Thus, the *rotr-1(ums53)* mutant recapitulates the changes in the lysosomal compartment that are observed during pathogen infection.

Both lysosomes and lysosome-related organelles stain positively for LysoTracker red in *C. elegans* intestinal tissues.[27-29] To determine which of these cellular compartments is affected in *rotr-1(ums53)* mutants, we used transgenic *C. elegans* strains with GFP markers specifically labeled for either lysosomes or lysosome-related organelles. For lysosomes, we used a GFP translational fusion for the protein LMP-1 (LMP-1::GFP), which is the *C. elegans* homolog of mammalian LAMP and CD68.[30] To label lysosome-related organelles, we used a GFP translational fusion for the protein PGP-2 (PGP-2::GFP), an ATP-binding cassette transporter that is expressed on the membranes of these vesicles.[27] Intriguingly, the size of PGP-2::GFP (+) vesicles (Figures 4C and 4D), but not LMP-1::GFP (+) vesicles (Figures S4C and S4D), was significantly smaller in *rotr-1(ums53)* mutants compared to wild-type animals. Of note, *tir-1(RNAi)* caused LMP-1::GFP (+) vesicles to increase in size in the *rotr-1(ums53)* mutant but not in the wild-type background (Figures S4C and S4D) for reasons that are unclear. As an orthologous approach to measure the size of lysosome-related organelles, we assessed autofluorescent granules in the blue channel (Figures S4E-S4G). We observed that the blue autofluorescent granules in the *rotr-1(ums53)* mutants were significantly smaller (Figures S4E and S4F) and fewer in number (Figures S4E and S4G) than in wild-type animals. These data are consistent with our findings using LysoTracker red (Figures 4A and 4B). Thus, the integrity of lysosome-related organelles, but not lysosomes, was compromised in *rotr-1(ums53)* mutants. This result is noteworthy considering our finding that TIR-1 is expressed on the membranes of lysosome-related organelles but not on lysosomes.[14]

Importantly, knockdown of *tir-1* did not rescue the collapsed PGP-2::GFP (+) vesicles in the *rotr-1(ums53)* mutants (Figures 4C and 4D). Thus, the condensation of lysosome-related organelles in *rotr-1* mutants occurred upstream of TIR-1. These data are important considering the findings in our companion study, which demonstrated that TIR-1 aggregates into puncta on the surface of condensed lysosome-related organelles to activate the p38 PMK-1 pathway.[14] Consistent with these observations, the hyperactivation of the p38 PMK-1-dependent immune reporter in *rotr-1(ums53)* mutants depended on the presence of lysosome-related organelles. RNAi-mediated knockdown of *pgp-2* (Figure 4E), but not *lmp-1* (Figure 4F), suppressed T24B8.5p::*gfp* activation in the *rotr-1(ums53)* mutants.

Thus, ROTR-1 supports the integrity of lysosome-related organelles, which suppresses positive feedback activation of p38 PMK-1 innate immunity.

ROTR-1 functions in the intestine to support lysosome-related organelle integrity, which restrains toxic propagation of p38 PMK-1 innate immunity

The *gfp*-based transcriptional reporter we generated for *rotr-1* revealed that this gene is expressed exclusively in the intestine, particularly in anterior and posterior intestinal epithelial cells (Figure 3K). To determine if *rotr-1* also functions in the intestine to

regulate the p38 PMK-1 pathway, we engineered *C. elegans* strains that expressed *rotr-1* under the control of promoters that directed its expression only in specific tissues. Endogenous expression of *rotr-1* under its own promoter suppressed the hyperactivation of T24B8.5p::*gfp* in the *rotr-1(ums53)* clean deletion mutant (Figure 5A), as we observed for *irg-5p::gfp* in the rescued *rotr-1(ums38)* mutant (Figure 2E). Intestinal expression of *rotr-1* (Figure 5B), but not neuronal (Figure 5C) or hypodermal expression (Figure 5D), suppressed the hyperactivation of T24B8.5p::*gfp* expression in *rotr-1(ums53)* mutants. We confirmed the tissue-specific expression of *rotr-1* in these strains using a construct that contains a split-leader mCherry sequence, which labeled the tissues with *rotr-1* expression (Figures 5B-5D).

We found that *rotr-1* loss-of-function mutants were hypersusceptible to killing by *P. aeruginosa* infection (Figure 5E), as we have observed with other mutants that also hyperactivate the p38 PMK-1 pathway.[12,17] Endogenous rescue of *rotr-1* under its own promoter restored resistance of *rotr-1(ums53)* null mutants against killing by *P. aeruginosa* (Figure 5E). Reintroduction of *rotr-1* in the intestine (Figure 5F), but not in the neurons (Figure 5G) or hypodermis (Figure 5H), rescued wild-type resistance to pathogen infection.

Our laboratory and others have previously shown that aberrant activation of the p38 PMK-1 pathway is deleterious to *C. elegans* growth and lifespan.[12,17,18,21,31,32] Consistent with these studies, *rotr-1(ums53)* mutants had a significantly reduced lifespan (Figure 6A) and delayed development as demonstrated by growth defects and decreased transition to the L4 larval stage (Figures 6B and 6C). Importantly, each of these defects in *rotr-1(ums53)* mutants was rescued in a *tir-1(qd4)* loss-of-function background (Figures 6A-6C), demonstrating that these effects were due to toxicities caused by hyperactivation of TIR-1.

We studied the contribution of lysosome-related organelle integrity to p38 PMK-1 immune regulation by performing developmental assays with the *pgp-2(kx48)* loss-of-function mutant (Figures 6D and 6E). PGP-2 is an ATP-binding cassette transporter expressed on the membranes of lysosome-related organelles and is required for their biogenesis.[27] RNAi of the p38 PMK-1 phosphatase *vhp-1*, which engages *tir-1* transcription in a positive feedback loop (Figure 1), triggers toxic activation of *tir-1* that delays *C. elegans* development (Figures 6D and 6E). Accordingly, *tir-1(RNAi)* suppressed the developmental delay of *vhp-1(RNAi)* animals (Figures 6D and 6E). Intriguingly, knockdown of *vhp-1* in the *pgp-2(kx48)* mutant was embryonically lethal, a phenotype that was suppressed by *tir-1(RNAi)* (Figures 6D and 6E). Thus, p38 PMK-1 immune pathway regulation by the lysosome-related organelle-TIR-1 axis is required for *C. elegans* development.

Together, these data demonstrate that lysosome-related organelle integrity, which is compromised in *rotr-1* mutants, restrains toxic positive feedback activation of p38 PMK-1 innate immunity by preventing aberrant TIR-1 aggregation.

DISCUSSION

Enzymatic TIR proteins have essential roles in innate immunity in bacteria, plants, and animals. Across the Tree of Life, members of this protein family oligomerize to initiate their intrinsic NAD^+ catalytic activity.[3,5,7,33,34] However, the mechanisms that control TIR protein multimerization are underexplored. In this study, we showed that the activity of TIR-1, the lone enzymatic TIR protein in *C. elegans*, is controlled through the maintenance of lysosome-related organelle integrity. Initially, we discovered that TIR-1 promotes its own activation by initiating a p38 PMK-1-dependent positive feedback loop, which drives the transcription, translation, and aggregation of TIR-1. Unchecked TIR-1 aggregation and activation decreased lifespan, reduced brood size, and stunted larval development. The previously uncharacterized protein ROTR-1 functions in intestinal tissues to maintain the integrity of the specific lysosomal compartment that expresses TIR-1, which restrains p38 PMK-1 innate immune activation by preventing aberrant TIR-1 aggregation.

In a companion study, we showed that TIR-1 is a pathogen sensor in *C. elegans* that is expressed on the surface of lysosome-related organelles.[14] We found that pyocyanin, a virulence effector secreted by the bacterial pathogen *P. aeruginosa*, alkalinized and condensed lysosome-related organelles, which caused TIR-1 to aggregate on their surface and activate the p38 PMK-1 pathway. Here, we found that *rotr-1* mutants recapitulated the contraction in size of lysosome-related organelles that we observed during pathogen infection, which drove pathological TIR-1 aggregation and p38 PMK-1 activation. Thus, we conclude that lysosome-related organelle integrity is maintained in *C. elegans* to prevent aberrant TIR-1 aggregation on the membranes of these organelles, which restrains toxic propagation of p38 innate immunity. Together, our companion studies demonstrate that the lysosomal-TIR-1-p38 axis functions in the pathogen effector-triggered activation of protective host immunity and is tightly regulated to promote intestinal immune homeostasis.[14]

We propose that p38 positive feedback potentiation of immune defenses promotes a rapid host response to pathogen infection. Concentration of TIR-1 into puncta, or higher-order oligomers, accelerates its enzymatic function.[8,12] It is therefore logical that positive feedback immune activation in *C. elegans* is caused by increasing the transcription and translation of TIR-1, which increases the likelihood of protein oligomerization. Perhaps not surprisingly, we found that excessive TIR-1 activity is detrimental to overall animal health. These data are consistent with findings from our group and others, which have demonstrated that chronic hyperactivation of the p38 PMK-1 pathway is toxic to nematodes.[17,35,36] We observed that hyperactivation of p38 PMK-1 in *rotr-1* mutants shortened nematode lifespan. In addition, *rotr-1* mutants were hypersusceptible to *P. aeruginosa* infection, a phenotype we have observed with other mutants that drive constitutive p38 PMK-1 pathway activation.[12] Thus, we attribute the enhanced susceptibility of *rotr-1* mutants to *P. aeruginosa* infection to the toxic effects of TIR-1 hyperactivation or other negative pleiotropies associated with the loss of lysosome-related organelle integrity.

Human SARM1 is expressed in neurons, where it promotes Wallerian degeneration of axon fragments following neuronal injury.[8,37-41] In this regard, SARM1 has emerged as

an attractive drug target to prevent pathologic neurodegeneration.[42] *C. elegans* TIR-1 has also been implicated in neuronal degeneration.[8,43] In this context, overexpression of TIR-1 promotes toxic axonal degeneration; however, what causes this toxicity is not known. Thus, an intriguing hypothesis is that lysosomal regulation of TIR-1 aggregation in neurons may mitigate TIR-1-induced neurotoxicity.

We demonstrated that ROTR-1 is required for the integrity of lysosome-related organelles, but it is not clear how ROTR-1 functions in this capacity. Our efforts to characterize the cell biology of ROTR-1 were unsuccessful given the inability to generate a functional tagged protein. Thus, we do not know if ROTR-1 is expressed on lysosome-related organelles, nor could we confirm *in vivo* the previous observation that ROTR-1 physically interacts with TIR-1. Nevertheless, our studies with *rotr-1* mutants characterized the importance of this specific cellular compartment in the regulation of the p38 PMK-1 immune pathway.

It is important to note that p38 PMK-1 promotes host adaptation to a multitude of exogenous and endogenous stresses.[10,12,15,18,19,22,44-49] In this regard, multiple different mechanisms have been identified that control the activity of this critically important cytoprotective kinase. The MAPK phosphatase *vhp-1* is a negative regulator of p38 PMK-1.[15] Several different amphid sensory neurons send signals to the intestine to suppress p38 PMK-1 activity.[18,50] Micronutrient deficiency primes p38 PMK-1 activation as part of an adaptive response to anticipate environmental threats during a time of relative vulnerability.[12] We propose here that each of these different mechanisms of p38 PMK-1 regulation are linked to cell biological mechanisms that are perturbed by the specific stressors that are surveilled to activate protective host defenses. In the case of the bacterial effector-triggered p38 immune activation induced by lysosomal damage, we demonstrated that the lysosomal compartment that expresses the activator of p38 is itself regulated to restrain exaggerated immune responses. Thus, we propose that mechanisms of pathogen detection—particularly effector-triggered immunity—evolved specific protective countermeasures to prevent unchecked immune activation.

RESOURCE AVAILABILITY

Lead contact

Further information and requests for resources or reagents should be directed to and will be fulfilled by the lead contact, Read Pukkila-Worley (read.pukkila-worley@umassmed.edu).

Materials availability

Strains and reagents generated in this study are available upon request.

Data and code availability

- The mRNA-seq datasets are available from the NCBI Gene Expression Omnibus using the accession number GEO: GSE256356 and will be publicly available as of the date of publication. All other data are available in the manuscript and the accompanying Table S3, which contains all source data and statistical tests used.
- This paper does not report original code.

- Any additional information required to reanalyze the data reported in this paper is available from the lead contact upon request.

STAR★METHODS

EXPERIMENTAL MODEL AND STUDY PARTICIPANT DETAILS

C. elegans strains—The previously published *C. elegans* strains used in this study were: N2 Bristol,[51] AU78 *agIs219* [T24B8.5p:*gfp::unc54*-3′UTR; *ttx-3*p::*gfp::unc-54*-3'UTR] *III*,[11] RPW403 *ums63* [TIR-1:wrmScarlet],[12] RPW386 *ums57* [TIR-1:3xFLAG]; *agIs219* [T24B8.5p:*gfp::unc54*-3′UTR; *ttx-3p::gfp::unc-54*-3′UTR] *III*,[12] MGH41 *alxIs1* [*vha-6*p::PGP-2:GFP; pRF4] (unpublished), RT258 *pwIs50* [LMP-1:GFP + Cbr-unc-119(+)].[54]

The strains developed in this study were: RPW446 *ums63* [TIR-1:wrmScarlet]; *rotr-1(ums53)*, RPW262 *acIs101* [pDB09.1(*irg-5p::gfp*); pRF4(*rol-6(su1006)*]; *rotr-1(ums33)*, RPW267 *acIs101* [pDB09.1(*irg-5p::gfp*); pRF4(*rol-6(su1006)*]; *rotr-1(ums38)*, RPW272 *acIs101* [pDB09.1(*irg-5p::gfp*); pRF4*(rol-6(su1006)]; rotr-1(ums39)*, RPW366 *acIs101* [pDB09.1(*irg-5p::gfp*); pRF4(*rol-6(su1006)]; rotr-1(ums53)*, RPW356 *agIs219* [T24B8.5p:*gfp::unc54*-3′UTR; *ttx-3p::gfp::unc-54*-3′UTR] *III*; *rotr-1(ums53)*, RPW384 *agIs219; rotr-1(ums53); umsEx78 [rotr-1*p::*rotr-1; myo-3*p::*mCherry*]_Line 1, RPW385 *agIs219; rotr-1(ums53); umsEx79* [*rotr-1*p:: *rotr-1*; *myo-3*p::*mCherry*]_Line 2, *C. elegans:* RPW415 *agIs219; rotr-1(ums53); umsEx83* [*vha-6*p::*rotr-1*::SL2:mCherry; *myo-3*p::mCherry]_Line 1, RPW416 *agIs219; rotr-1 (ums53); umsEx84* [*vha-6*p::*rotr-1*::SL2:mCherry; *myo-3*p::mCherry]_Line 2, RPW417 *agIs219; rotr-1(ums53); umsEx85* [*sng-1*p::*rotr-1*::SL2:mCherry; *myo-3*p::mCherry]_Line 1, RPW418 *agIs219; rotr-1 (ums53); umsEx86* [*sng-1*p::*rotr-1*::SL2:mCherry; *myo-3*p::mCherry]_Line 2, RPW419 *agIs219; rotr-1 (ums53); umsEx87* [*sng-1*p::*rotr-1*::SL2:mCherry; *myo-3*p::mCherry]_Line 3, RPW442 *agIs219; rotr-1(ums53); umsEx95* [*col-10*p::*rotr-1*::SL2:mCherry; *myo*-3p::mCherry]_Line 1, RPW443 *agIs219; rotr-1(ums53); umsEx96* [*col-10*p::*rotr-1*::SL2:mCherry; *myo-3*p::mCherry]_Line 2, RPW444 *agIs219; rotr-1(ums53); umsEx97* [*col-10*p::*rotr-1*::SL2:mCherry; *myo-3*p::mCherry]_Line 3, RPW398 *umsEx132* [*rotr-1*p::*gfp; myo-3*p::mCherry], RPW420 *rotr-1(ums53); ums57* [TIR-1:3xFLAG]; *agIs219*, RPW447 *ums81* [ROTR-1:3xHA]; *agIs219*, RPW471 *ums75* [3xFLAG::ROTR-1]; *agIs219*, RPW527 *alxIs1* [*vha-6*p::PGP-2:GFP; pRF4(*rol-6(su1006)];tir-1(ums63); rotr-1(ums53)*, and RPW526 *pwIs50* [LMP-1:GFP + Cbr-unc-119(+)];*tir-1(ums63); rotr-1(ums53)*.

C. elegans* growth conditions—C. elegans* strains were maintained on standard nematode growth medium (NGM) plates [0.25% Bacto-peptone, 0.3% sodium chloride, 1.7% agar (Fisher agar), 5 μg/mL cholesterol, 25 mM potassium phosphate pH 6.0, 1 mM magnesium sulfate, 1 mM calcium chloride] with *E. coli* OP50 as a food source, as described.[51]

Bacterial strains—Bacteria used in this study were *Escherichia coli (E. coli)* OP50,[51] *E. coli* HT115(DE3),[52] and *Pseudomonas aeruginosa* strain PA14.[53]

Bacterial growth conditions—*E. coli* OP50 was grown in LB broth supplemented with 0.175 mg/mL streptomycin at 37°C for 16–18 h at 250 rpm. *P. aeruginosa* strain PA14 was grown in LB broth at 37°C for 14–15 h at 250 rpm.

METHOD DETAILS

Identification of *rotr-1* through an unbiased *irg-5* forward genetic screen —Ethyl methanesulfonate (EMS) mutagenesis was performed on strain *acIs101* (*irg-5*p::*gfp*).[17,18] Briefly, synchronized L4 animals were treated with 48.6 mM EMS in M9 liquid for 4 h at 22°C on a roller. P0 animals were plated onto NGM plates with *E. coli* OP50. Gravid F1 progeny were then treated with hypochlorite and eggs were allowed to hatch overnight. Synchronized F2 progeny were grouped into 7 genetically distinct pools and screened for bright and constitutive GFP expression. Approximately 33,000 haploid genomes from the F2 generation were screened. Animals with significant developmental delay were excluded. From this screen, 9 mutants were identified. Forward genetic mutants *ums33* and *ums39* came from the same pool and *ums38* came from a separate pool.

Mutants were backcrossed with the parent strain (*acIs101*) twice. Progeny from each mutant, unbackcrossed and backcrossed, were then pooled. Genomic DNA from the pooled recombinants and parent strain were isolated using the Gentra Puregene DNA isolation kit (Qiagen) and sent for whole-genome sequencing (BGI). Animals were sequenced on the DNBseq platform with 100 bp paired-end runs. Each sample had an average of 65 million reads with a final coverage of around 130x.

Homozygous variants from the WBcel235 (ce11) *C. elegans* reference genome that were present in the unbackcrossed and backcrossed mutants, but not in the parent strain *acIs101* strain, were identified using in-house scripts. In brief, homozygous variants were called using ‘bcftools’. Any variants that were identified in both the parent *acIs101* strain and the forward genetic mutants were removed using ‘bedtools’. Finally, homozygous variants were annotated using ‘snpEff’ with *C. elegans* reference genome WBcel235.99.

***C. elegans* strain construction—**CRISPR-Cas9 editing with single-stranded oligodeoxynucleotide (ssODN) homology-directed repair was used to generate *rotr-1(ums53)* and ROTR-1 epitope-tagged strains.[67] All CRISPR reagents were purchased from Integrated DNA Technologies. Target guide sequences were selected using the CHOPCHOP web tool. The ssODN repair templates contained indicated deletions with 35 bp flanking homology arms. ssODN sequences are listed in Table S4. The F1 progeny were screened for Rol (roller) phenotypes 3 to 4 days after injection and then for indicated edits using PCR and Sanger sequencing. Primer sequences used for genotyping are listed in Table S4.

Generation of transgenic rescue strains was performed as follows.[18,20] For endogenous transgenic rescue of *rotr-1*, the *rotr-1* promoter (~2 kb upstream of the ATG start codon), *rotr-1*, and the 5′ and 3′ untranslated regions (UTRs) were amplified and cloned into a pUC19 vector. The plasmid was then microinjected at 25 ng/μL with 5 ng/μL of pCFJ104 (*myo-3*p::*mCherry::unc54*) and 120 ng/μL of empty pUC19 plasmid. For tissue-specific transgenic rescue strains, the *rotr-1* gene, including both the 5′ and 3′ UTRs was fused to

either the *col-10* promoter (for hypodermal rescue), *vha-6* promoter (for intestinal rescue), or the *sng-1* promoter (for pan-neuronal rescue) via Gibson assembly. Plasmids were then microinjected into the *rotr-1(ums53); agIs219* mutants at 10 ng/μL with 5 ng/μL pCFJ104 (*myo-3*p::*mCherry::unc-54*) and 135 ng/μL empty pUC19 plasmid.

Feeding RNAi—*C. elegans* were fed *E. coli* HT115 expressing dsRNA targeting the genes of interest with modifications.[52,68,69] In brief, HT115 bacteria expressing specific dsRNA were grown on LB agar containing 50 μg/mL ampicillin and 15 μg/mL tetracycline at 37°C overnight. Colonies were then inoculated in LB broth containing 50 μg/mL ampicillin overnight at 37°C for 16–18 h with shaking at 250 rpm. Overnight cultures were then seeded onto NGM plates containing 5 mM IPTG and 50 μg/mL carbenicillin and incubated for 16–18 h at 37°C. Synchronized L1 animals were then transferred onto NGM plates with the grown bacteria and allowed to mature to the L4 stage.

For Figures 4G and 4H, *C. elegans* animals were treated with two-generation RNAi. Animals were first allowed to mature from L1 to gravid adults on individual RNAi clones and then treated with hypochlorite to release eggs. Eggs were allowed to hatch overnight and synchronized L1s were dropped onto the same RNAi clones that their parents were grown on.

LysoTracker red assays—Animals were stained with LysoTracker red (Thermo Fisher) as previously described.[27,28] To stain animals with LysoTracker red, 60 mm NGM plates (about 10 mL media) were first seeded with *E. coli* OP50 or HT115 and allowed to dry. Stocks were then diluted 1:10 in M9W (100 μM). 100 μL of each dye was then added on top of the dried bacteria and the dye was allowed to percolate through the plates for 1–2 h (final concentration 1 μM). L1 synchronized animals were then dropped on NGM plates containing either 1–2% DMSO or 1 μM LysoTracker red and allowed to grow in the dark until the L4 stage. About 1–2 h before imaging, animals were transferred to NGM plates containing freshly seeded *E. coli* OP50. Stained animals were visualized using the Zeiss AXIO Imager Z2 microscope with a Zeiss Axiocam 506 mono camera and Zen 2.5 (Zeiss) software.

Microscopy and image analysis—For GFP fluorescence imaging, nematodes were mounted onto 2% agarose pads, paralyzed with 50 mM tetramisole (Sigma), and imaged using a Zeiss AXIO Imager Z2 microscope with a Zeiss Axiocam 506 mono camera and Zen 2.5 (Zeiss) software. For TIR-1:wrmScarlet imaging in Figure 1D, animals were mounted onto 2% agarose pads, paralyzed with 50 mM tetramisole (Sigma), and sealed with coverslips and VALAP (a 1:1:1 mixture of Vaseline, lanolin, and paraffin). Slides were then inverted and imaged on the THUNDER Imager (Leica DMi8, inverted microscope) with a Leica 63× objective and LasX software (Leica). For Figure 4A, animals were imaged using the Zeiss AXIO Imager Z2 microscope with a Zeiss Axiocam 506 mono camera and Zen 2.5 (Zeiss) software.

TIR-1:wrmScarlet puncta quantification was performed as described previously.[12]—For Figures 4C-4F, animals were imaged on the THUNDER Imager (Leica) and images were deconvoluted with Thunder. The diameter of PGP-2:GFP and

LMP-1:GFP vesicles were then quantified on ImageJ (Fiji). For each animal, about 10 GFP+ vesicles were randomly identified in the last intestinal cell pair. The vesicular diameters were determined by using the line tool across the widest part of each vesicle. The measured diameters for each animal were averaged and displayed as a single data point. Source data can be found in Table S3.

Gene expression analyses and bioinformatics—RNA-sequencing and data analysis were performed as follows.[12,70] Briefly, synchronized wild-type T24B8.5p:*gfp* or *rotr-1(ums53)*;T24B8.5p:*gfp* L1 stage *C. elegans* were grown to the L4 stage on NGM plates seeded with *E. coli* OP50. At the L4 stage, animals were then washed to "slow-kill" plates containing *E. coli* OP50 or *P. aeruginosa* PA14. Animals were exposed to each condition for 4 h at 25°C. Animals were then harvested by washing with M9 multiple times before RNA was isolated using TriReagent (Sigma-Aldrich), column purified (Qiagen), and analyzed by 100 bp paired-end mRNA-sequencing using the BGISEQ-500 platform (BGIAmericasCorp) with >20 million reads per sample. The quality of raw sequencing data was evaluated by FastQC (version 0.11.5), and clean reads were aligned to the *C. elegans* reference genome (WBcel235) and quantified using Kallisto (version 0.45.0).[58] Differentially expressed genes were identified using Sleuth (version 0.30.0).[59] Pearson correlation statistical analysis was performed using Prism 10. Gene set enrichment analysis of RNA-seq was performed using WormCat[61] for annotation of *C. elegans* gene categories and GSEA (version 4.2.3).[60] For GSEA, each differentially regulated gene was given a π-value.[25] The π-value was calculated as:

$$\pi = \phi \times (- log_{10} p)$$

where ϕ equals $\log_2$(fold-change) and p equals the p-value. Genes were then preranked from the highest π value to the lowest π value.

For qRT-PCR studies, RNA was extracted from about 3000 L4 animals and reverse transcribed to cDNA using the iScript cDNA Synthesis Kit (Bio-Rad). cDNA was then analyzed on the CFX384 thermocycler (Bio-Rad) with primers described in Table S4. All values were normalized to the geometric mean of the housekeeping control genes *act-3* and *snb-1*. Relative expression was then calculated using the Pfaffl method.[71]

Immunoblot analyses—Protein lysates were prepared using a Teflon Dounce homogenizer from 50,000–10,000 *C elegans* animals grown to the L4 larval stage on NGM plates seeded with *E. coli* OP50.[12,70] LDS Sample Buffer (Thermo Fisher Scientific) was added to a concentration of 1X with 5% β-mercaptoethanol. All samples were incubated at 70°C for 10 min. Total protein from each sample was resolved on NuPage Bis-Tris 4–12% gels (Invitrogen), for detection of phosphorylated p38 PMK-1, total p38 PMK-1 and ROTR-1, or NuPage Tris-Acetate 3–8% gels (Invitrogen), for detection of TIR-1:3xFLAG. Protein was then transferred to 0.2 mM nitrocellulose membranes (Bio-Rad) and blocked with 5% milk in 1x TBS +0.2% Tween 20 for 1 h. Blots were then probed with a 1:1000 dilution of mouse monoclonal anti-FLAG M2 (Sigma, #F1804), 1:1000 phospho p38 PMK-1 (Cell Signaling Technology, #9211), 1:1000 total PMK-1,[24] 1:2000 mouse

monoclonal anti-alpha-Tubulin (Sigma, #T5168), overnight at 4°C. A polyclonal antibody against the ROTR-1 protein was raised using the peptide LDRSPPSDDGTQKV (ROTR-1 amino acids 288 to 301) in rabbit (Thermo Fisher Scientific). Anti-ROTR-1 sera was used at a dilution of 1:1000. We confirmed that anti-ROTR-1 sera was specific for ROTR-1 using *rotr-1(ums53)* (Figure S2B). For detection of 3xFLAG-tagged ROTR-1, blots were probed with 1:500 dilution of mouse monoclonal anti-FLAG M2. For detection of 3xHA-tagged ROTR-1, blots were probed with 1:500 anti-HA (Roche, #11867423001). Anti-mouse IgG-HRP (Abcam, #ab6789), anti-rabbit IgG-HRP (Cell Signaling Technology, #7074), or anti-rat IgG-HRP (Abcam, #ab97057) secondary antibodies were used at a dilution of 1:10,000 to detect primary antibodies. Blots were then developed with the addition of SuperSignal West Pico or West Femto PLUS Chemiluminescent Substrate (Thermo Fisher Scientific) and visualized using a ChemiDoc MP Imaging System (Bio-Rad). Band intensities were quantified using ImageJ (Fiji).

For NativePAGE analysis, protein lysates were prepared in 1x NativePAGE buffer (Invitrogen), 1% digitonin, and HALT protease inhibitor (Thermo Fisher). Coomassie G-250 additive was added to samples and loaded onto NativePAGE 3–12% Bis-Tris gels (Invitrogen). Samples were first run in dark blue cathode buffer (inner chamber) until the front ran 1/3 down the gel. The buffer was then switched to the light blue cathode buffer. Protein was then transferred onto 0.2 μm PVDF membranes overnight at 4°C. After transfer, membranes were placed in 8% acetic acid and fixed for 15 min at room temperature on a rocker. The blot was then destained with 50% methanol/10% acetic acid until the membrane was white and blocked with 5% milk in 1x TBS +0.2% Tween 20 for 1 h at room temperature on a rocker. Blots were then transferred to mouse anti-FLAG M2 (Sigma, #F1804) antibody overnight at 4°C. The following day, blots were washed and transferred to anti-mouse IgG-HRP (Abcam, #ab6789) for 1 h at room temperature on a rocker. Blots were then developed with the addition of SuperSignal West Femto PLUS Chemiluminescent Substrate (Thermo Fisher Scientific) and visualized using a ChemiDoc MP Imaging System (Bio-Rad).

Development and lifespan assays—Around 200 synchronized L1 animals were grown on *E. coli* OP50 for 48 h at 20°C. Larval stages were then visually quantified under a dissecting microscope. Animals older than the L4 stage were identified and the percent L4+ was calculated.[17,18] Each genotype had four biological replicates. All source data can be found in Table S3.

For lifespan assays, L4 animals from each genotype were transferred onto NGM plates containing 0.1 mg/mL 5-fluorodeoxyuridine (FUDR), to prevent progeny from hatching, and grown at 20°C. Live animals were scored daily until all animals on each plate died. Any plates with visible contamination were removed from the analysis. Sample size (n), mean lifespan and statistics can be found in Table S1.

***C. elegans* pathogenesis assays—**"Slow-killing" *P. aeruginosa* infection experiments were performed as previously described.[72] In brief, *P. aeruginosa* was grown as described above and 10 μL overnight culture was spread onto the center of 35-mm tissue culture plates containing 4 mL slow-kill agar (0.35% Bacto-peptone, 0.3% sodium chloride, 1.7%

agar, 5 μg/mL cholesterol, 25 mM potassium phosphate, 1 mM magnesium sulfate, 1 mM calcium chloride). Plates were then incubated for 24 h at 37°C followed by 24 h at 25°C. *C. elegans* animals at the L4 larval stage were then transferred to *P. aeruginosa* slow-kill plates containing 0.1 mg/mL FUDR. Dead animals were scored twice daily until completion. Three trials of the assay were performed. Sample sizes, mean survival, and p-values for all trials are shown in Table S1.

QUANTIFICATION AND STATISTICAL ANALYSIS

Differences in the survival of *C. elegans* in the *P. aeruginosa* pathogenesis assays or lifespan assays were determined with the log rank test after survival curves were estimated for each group with the Kaplan-Meier method. OASIS 2 was used for these statistical analyses.[56] Statistical hypothesis testing was performed with Prism 10 (GraphPad Software) using methods indicated in the figure legends. Table S3 contains all source data and statistical analysis methods and results. Sample sizes, survival, and *p*-values for all trials are shown in Table S1.

Supplementary Material

Refer to Web version on PubMed Central for supplementary material.

ACKNOWLEDGMENTS

The authors thank Melanie Trombly for insightful comments on the manuscript. The authors also thank Alexander Soukas for kindly sharing the PGP-2::GFP strain. The research was supported by R01 AI130289 (to R.P.-W.), R01 AI159159 (to R.P.-W.), R21 AI163430 (to R.P.-W.), F30 DK127690 (to S.Y.T.-K.), T32 AI095213 (to S.Y.T.-K.), and T32 GM107000 (to S.Y.T.-K.). Some strains were provided by the *Caenorhabditis* Genetics Center, which is funded by the NIH Office of Research Infrastructure Programs (P40 OD010440). The funders had no role in study design, data collection and analysis, decision to publish, or preparation of the manuscript.

REFERENCES

1. Essuman K, Summers DW, Sasaki Y, Mao X, DiAntonio A, and Milbrandt J (2017). The SARM1 Toll/Interleukin-1 Receptor Domain Possesses Intrinsic NAD(+) Cleavage Activity that Promotes Pathological Axonal Degeneration. Neuron 93, 1334–1343.e5. 10.1016/j.neuron.2017.02.022. [PubMed: 28334607]
2. Wan L, Essuman K, Anderson RG, Sasaki Y, Monteiro F, Chung EH, Osborne Nishimura E, DiAntonio A, Milbrandt J, Dangl JL, and Nishimura MT (2019). TIR domains of plant immune receptors are NAD(+)-cleaving enzymes that promote cell death. Science 365, 799–803. 10.1126/science.aax1771. [PubMed: 31439793]
3. Morehouse BR, Govande AA, Millman A, Keszei AFA, Lowey B, Ofir G, Shao S, Sorek R, and Kranzusch PJ (2020). STING cyclic dinucleotide sensing originated in bacteria. Nature 586, 429–433. 10.1038/s41586-020-2719-5. [PubMed: 32877915]
4. Doron S, Melamed S, Ofir G, Leavitt A, Lopatina A, Keren M, Amitai G, and Sorek R (2018). Systematic discovery of antiphage defense systems in the microbial pangenome. Science 359, eaar4120. 10.1126/science.aar4120. [PubMed: 29371424]
5. Ma S, Lapin D, Liu L, Sun Y, Song W, Zhang X, Logemann E, Yu D, Wang J, Jirschitzka J, et al. (2020). Direct pathogen-induced assembly of an NLR immune receptor complex to form a holoenzyme. Science 370, eabe3069. 10.1126/science.abe3069. [PubMed: 33273071]
6. Martin R, Qi T, Zhang H, Liu F, King M, Toth C, Nogales E, and Staskawicz BJ (2020). Structure of the activated ROQ1 resistosome directly recognizing the pathogen effector XopQ. Science 370, eabd9993. 10.1126/science.abd9993. [PubMed: 33273074]

7. Sporny M, Guez-Haddad J, Lebendiker M, Ulisse V, Volf A, Mim C, Isupov MN, and Opatowsky Y (2019). Structural Evidence for an Octameric Ring Arrangement of SARM1. J. Mol. Biol 431, 3591–3605. 10.1016/j.jmb.2019.06.030. [PubMed: 31278906]
8. Loring HS, Czech VL, Icso JD, O'Connor L, Parelkar SS, Byrne AB, and Thompson PR (2021). A phase transition enhances the catalytic activity of SARM1, an NAD(+) glycohydrolase involved in neurodegeneration. Elife 10, e66694. 10.7554/eLife.66694. [PubMed: 34184985]
9. Liberati NT, Fitzgerald KA, Kim DH, Feinbaum R, Golenbock DT, and Ausubel FM (2004). Requirement for a conserved Toll/interleukin-1 resistance domain protein in the *Caenorhabditis elegans* immune response. Proc. Natl. Acad. Sci. USA 101, 6593–6598. 10.1073/pnas.0308625101. [PubMed: 15123841]
10. Troemel ER, Chu SW, Reinke V, Lee SS, Ausubel FM, and Kim DH (2006). p38 MAPK regulates expression of immune response genes and contributes to longevity in *C. elegans*. PLoS Genet. 2, e183. 10.1371/journal.pgen.0020183. [PubMed: 17096597]
11. Shivers RP, Kooistra T, Chu SW, Pagano DJ, and Kim DH (2009). Tissue-specific activities of an immune signaling module regulate physiological responses to pathogenic and nutritional bacteria in *C. elegans*. Cell Host Microbe 6, 321–330. 10.1016/j.chom.2009.09.001. [PubMed: 19837372]
12. Peterson ND, Icso JD, Salisbury JE, Rodríguez T, Thompson PR, and Pukkila-Worley R (2022). Pathogen infection and cholesterol deficiency activate the C. elegans p38 immune pathway through a TIR-1/SARM1 phase transition. Elife 11, e74206. 10.7554/eLife.74206. [PubMed: 35098926]
13. Khazma T, Grossman A, Guez-Haddad J, Feng C, Dabas H, Sain R, Weitman M, Zalk R, Isupov MN, Hammarlund M, et al. (2023). Structure-function analysis of ceTIR-1/hSARM1 explains the lack of Wallerian axonal degeneration in C. elegans. Cell Rep. 42, 113026. 10.1016/j.celrep.2023.113026. [PubMed: 37635352]
14. Tse-Kang SY, Wani KA, Peterson ND, Page A, Humphries F, and Pukkila-Worley R (2024). Intestinal immunity in *C. elegans* is activated by pathogen effector-triggered aggregation of the guard protein TIR-1 on lysosome-related organelles. Immunity 57, 5399. 10.1016/j.immuni.2024.08.013.
15. Kim DH, Liberati NT, Mizuno T, Inoue H, Hisamoto N, Matsumoto K, and Ausubel FM (2004). Integration of Caenorhabditis elegans MAPK pathways mediating immunity and stress resistance by MEK-1 MAPK kinase and VHP-1 MAPK phosphatase. Proc. Natl. Acad. Sci. USA 101, 10990–10994. 10.1073/pnas.0403546101. [PubMed: 15256594]
16. Mizuno T, Hisamoto N, Terada T, Kondo T, Adachi M, Nishida E, Kim DH, Ausubel FM, and Matsumoto K (2004). The *Caenorhabditis elegans* MAPK phosphatase VHP-1 mediates a novel JNK-like signaling pathway in stress response. EMBO J. 23, 2226–2234. 10.1038/sj.emboj.7600226. [PubMed: 15116070]
17. Cheesman HK, Feinbaum RL, Thekkiniath J, Dowen RH, Conery AL, and Pukkila-Worley R (2016). Aberrant Activation of p38 MAP Kinase-Dependent Innate Immune Responses Is Toxic to *Caenorhabditis elegans*. G3 (Bethesda) 6, 541–549. 10.1534/g3.115.025650. [PubMed: 26818074]
18. Foster KJ, Cheesman HK, Liu P, Peterson ND, Anderson SM, and Pukkila-Worley R (2020). Innate Immunity in the C. elegans Intestine Is Programmed by a Neuronal Regulator of AWC Olfactory Neuron Development. Cell Rep. 31, 107478. 10.1016/j.celrep.2020.03.042. [PubMed: 32268082]
19. Wu Z, Isik M, Moroz N, Steinbaugh MJ, Zhang P, and Blackwell TK (2019). Dietary Restriction Extends Lifespan through Metabolic Regulation of Innate Immunity. Cell Metab. 29, 1192–1205.e8. 10.1016/j.cmet.2019.02.013. [PubMed: 30905669]
20. Torzone SK, Park AY, Breen PC, Cohen NR, and Dowen RH (2023). Opposing action of the FLR-2 glycoprotein hormone and DRL-1/FLR-4 MAP kinases balance p38-mediated growth and lipid homeostasis in C. elegans. PLoS Biol. 21, e3002320. 10.1371/journal.pbio.3002320. [PubMed: 37773960]
21. Kim KW, Thakur N, Piggott CA, Omi S, Polanowska J, Jin Y, and Pujol N (2016). Coordinated inhibition of C/EBP by Tribbles in multiple tissues is essential for Caenorhabditis elegans development. BMC Biol. 14, 104. 10.1186/s12915-016-0320-z. [PubMed: 27927209]
22. Pukkila-Worley R, Feinbaum R, Kirienko NV, Larkins-Ford J, Conery AL, and Ausubel FM (2012). Stimulation of host immune defenses by a small molecule protects C. elegans from bacterial infection. PLoS Genet. 8, e1002733. 10.1371/journal.pgen.1002733. [PubMed: 22719261]

23. Anderson SM, and Pukkila-Worley R (2020). Immunometabolism in Caenorhabditis elegans. PLoS Pathog. 16, e1008897. 10.1371/journal.ppat.1008897. [PubMed: 33031414]
24. Peterson ND, Cheesman HK, Liu P, Anderson SM, Foster KJ, Chhaya R, Perrat P, Thekkiniath J, Yang Q, Haynes CM, and Pukkila-Worley R (2019). The nuclear hormone receptor NHR-86 controls anti-pathogen responses in C. elegans. PLoS Genet. 15, e1007935. 10.1371/journal.pgen.1007935. [PubMed: 30668573]
25. Xiao Y, Hsiao TH, Suresh U, Chen HIH, Wu X, Wolf SE, and Chen Y (2014). A novel significance score for gene selection and ranking. Bioinformatics 30, 801–807. 10.1093/bioinformatics/btr671. [PubMed: 22321699]
26. Li S, Armstrong CM, Bertin N, Ge H, Milstein S, Boxem M, Vidalain PO, Han JDJ, Chesneau A, Hao T, et al. (2004). A map of the interactome network of the metazoan C. elegans. Science 303, 540–543. 10.1126/science.1091403. [PubMed: 14704431]
27. Hermann GJ, Schroeder LK, Hieb CA, Kershner AM, Rabbitts BM, Fonarev P, Grant BD, and Priess JR (2005). Genetic analysis of lysosomal trafficking in Caenorhabditis elegans. Mol. Biol. Cell 16, 3273–3288. 10.1091/mbc.e05-01-0060. [PubMed: 15843430]
28. Soukas AA, Carr CE, and Ruvkun G (2013). Genetic regulation of Caenorhabditis elegans lysosome related organelle function. PLoS Genet. 9, e1003908. 10.1371/journal.pgen.1003908. [PubMed: 24204312]
29. O'Rourke EJ, Soukas AA, Carr CE, and Ruvkun G (2009). C. elegans major fats are stored in vesicles distinct from lysosome-related organelles. Cell Metab. 10, 430–435. 10.1016/j.cmet.2009.10.002. [PubMed: 19883620]
30. Kostich M, Fire A, and Fambrough DM (2000). Identification and molecular-genetic characterization of a LAMP/CD68-like protein from Caenorhabditis elegans. J. Cell Sci 113, 2595–2606. 10.1242/jcs.113.14.2595. [PubMed: 10862717]
31. Richardson CE, Kooistra T, and Kim DH (2010). An essential role for XBP-1 in host protection against immune activation in *C. elegans*. Nature 463, 1092–1095. 10.1038/nature08762. [PubMed: 20182512]
32. Sun J, Singh V, Kajino-Sakamoto R, and Aballay A (2011). Neuronal GPCR controls innate immunity by regulating noncanonical unfolded protein response genes. Science 332, 729–732. 10.1126/science.1203411. [PubMed: 21474712]
33. Shi Y, Kerry PS, Nanson JD, Bosanac T, Sasaki Y, Krauss R, Saikot FK, Adams SE, Mosaiab T, Masic V, et al. (2022). Structural basis of SARM1 activation, substrate recognition, and inhibition by small molecules. Mol. Cell 82, 1643–1659.e10. 10.1016/j.molcel.2022.03.007. [PubMed: 35334231]
34. Essuman K, Milbrandt J, Dangl JL, and Nishimura MT (2022). Shared TIR enzymatic functions regulate cell death and immunity across the tree of life. Science 377, eabo0001. 10.1126/science.abo0001. [PubMed: 35857622]
35. Nhan JD, Turner CD, Anderson SM, Yen CA, Dalton HM, Cheesman HK, Ruter DL, Uma Naresh N, Haynes CM, Soukas AA, et al. (2019). Redirection of SKN-1 abates the negative metabolic outcomes of a perceived pathogen infection. Proc. Natl. Acad. Sci. USA 116, 22322–22330. 10.1073/pnas.1909666116. [PubMed: 31611372]
36. Weaver BP, Weaver YM, Omi S, Yuan W, Ewbank JJ, and Han M (2020). Non-Canonical Caspase Activity Antagonizes p38 MAPK Stress-Priming Function to Support Development. Dev. Cell 53, 358–369.e6. 10.1016/j.devcel.2020.03.015. [PubMed: 32302544]
37. Osterloh JM, Yang J, Rooney TM, Fox AN, Adalbert R, Powell EH, Sheehan AE, Avery MA, Hackett R, Logan MA, et al. (2012). dSarm/Sarm1 is required for activation of an injury-induced axon death pathway. Science 337, 481–484. 10.1126/science.1223899. [PubMed: 22678360]
38. Gerdts J, Brace EJ, Sasaki Y, DiAntonio A, and Milbrandt J (2015). SARM1 activation triggers axon degeneration locally via NAD(+) destruction. Science 348, 453–457. 10.1126/science.1258366. [PubMed: 25908823]
39. Gerdts J, Summers DW, Sasaki Y, DiAntonio A, and Milbrandt J (2013). Sarm1-mediated axon degeneration requires both SAM and TIR interactions. J. Neurosci 33, 13569–13580. 10.1523/jneurosci.1197-13.2013. [PubMed: 23946415]

40. Henninger N, Bouley J, Sikoglu EM, An J, Moore CM, King JA, Bowser R, Freeman MR, and Brown RH Jr. (2016). Attenuated traumatic axonal injury and improved functional outcome after traumatic brain injury in mice lacking Sarm1. Brain 139, 1094–1105. 10.1093/brain/aww001. [PubMed: 26912636]
41. Geisler S, Doan RA, Strickland A, Huang X, Milbrandt J, and DiAntonio A (2016). Prevention of vincristine-induced peripheral neuropathy by genetic deletion of SARM1 in mice. Brain 139, 3092–3108. 10.1093/brain/aww251. [PubMed: 27797810]
42. Loring HS, and Thompson PR (2020). Emergence of SARM1 as a Potential Therapeutic Target for Wallerian-type Diseases. Cell Chem. Biol 27, 1–13. 10.1016/j.chembiol.2019.11.002. [PubMed: 31761689]
43. Czech VL, O'Connor LC, Philippon B, Norman E, and Byrne AB (2023). TIR-1/SARM1 inhibits axon regeneration and promotes axon degeneration. Elife 12, e80856. 10.7554/eLife.80856. [PubMed: 37083456]
44. Bolz DD, Tenor JL, and Aballay A (2010). A conserved PMK-1/p38 MAPK is required in caenorhabditis elegans tissue-specific immune response to Yersinia pestis infection. J. Biol. Chem 285, 10832–10840. 10.1074/jbc.M109.091629. [PubMed: 20133945]
45. Irazoqui JE, Urbach JM, and Ausubel FM (2010). Evolution of host innate defence: insights from *Caenorhabditis elegans* and primitive invertebrates. Nat. Rev. Immunol 10, 47–58. 10.1038/nri2689. [PubMed: 20029447]
46. Ding W, Smulan LJ, Hou NS, Taubert S, Watts JL, and Walker AK (2015). s-Adenosylmethionine Levels Govern Innate Immunity through Distinct Methylation-Dependent Pathways. Cell Metab. 22, 633–645. 10.1016/j.cmet.2015.07.013. [PubMed: 26321661]
47. McCallum KC, and Garsin DA (2016). The Role of Reactive Oxygen Species in Modulating the Caenorhabditis elegans Immune Response. PLoS Pathog. 12, e1005923. 10.1371/journal.ppat.1005923. [PubMed: 27832190]
48. Goh GYS, Winter JJ, Bhanshali F, Doering KRS, Lai R, Lee K, Veal EA, and Taubert S (2018). NHR-49/HNF4 integrates regulation of fatty acid metabolism with a protective transcriptional response to oxidative stress and fasting. Aging Cell 17, e12743. 10.1111/acel.12743. [PubMed: 29508513]
49. Fanelli MJ, Welsh CM, Lui DS, Smulan LJ, and Walker AK (2023). Immunity-linked genes are stimulated by a membrane stress pathway linked to Golgi function and the ARF-1 GTPase. Sci. Adv 9, eadi5545. 10.1126/sciadv.adi5545. [PubMed: 38055815]
50. An JH, and Blackwell TK (2003). SKN-1 links C. elegans mesendodermal specification to a conserved oxidative stress response. Genes Dev. 17, 1882–1893. 10.1101/gad.1107803. [PubMed: 12869585]
51. Brenner S. (1974). The genetics of Caenorhabditis elegans. Genetics 77, 71–94. [PubMed: 4366476]
52. Fire A, Xu S, Montgomery MK, Kostas SA, Driver SE, and Mello CC (1998). Potent and specific genetic interference by double-stranded RNA in Caenorhabditis elegans. Nature 391, 806–811. 10.1038/35888. [PubMed: 9486653]
53. Rahme LG, Stevens EJ, Wolfort SF, Shao J, Tompkins RG, and Ausubel FM (1995). Common virulence factors for bacterial pathogenicity in plants and animals. Science 268, 1899–1902. [PubMed: 7604262]
54. Treusch S, Knuth S, Slaugenhaupt SA, Goldin E, Grant BD, and Fares H (2004). Caenorhabditis elegans functional orthologue of human protein h-mucolipin-1 is required for lysosome biogenesis. Proc. Natl. Acad. Sci. USA 101, 4483–4488. 10.1073/pnas.0400709101. [PubMed: 15070744]
55. Schindelin J, Arganda-Carreras I, Frise E, Kaynig V, Longair M, Pietzsch T, Preibisch S, Rueden C, Saalfeld S, Schmid B, et al. (2012). Fiji: an open-source platform for biological-image analysis. Nat. Methods 9, 676–682. 10.1038/nmeth.2019. [PubMed: 22743772]
56. Han SK, Lee D, Lee H, Kim D, Son HG, Yang JS, Lee SJV, and Kim S (2016). OASIS 2: online application for survival analysis 2 with features for the analysis of maximal lifespan and healthspan in aging research. Oncotarget 7, 56147–56152. 10.18632/oncotarget.11269. [PubMed: 27528229]

57. Labun K, Montague TG, Krause M, Torres Cleuren YN, Tjeldnes H, and Valen E (2019). CHOPCHOP v3: expanding the CRISPR web toolbox beyond genome editing. Nucleic Acids Res. 47, W171–W174. 10.1093/nar/gkz365. [PubMed: 31106371]
58. Bray NL, Pimentel H, Melsted P, and Pachter L (2016). Near-optimal probabilistic RNA-seq quantification. Nat. Biotechnol 34, 525–527. 10.1038/nbt.3519. [PubMed: 27043002]
59. Pimentel H, Bray NL, Puente S, Melsted P, and Pachter L (2017). Differential analysis of RNA-seq incorporating quantification uncertainty. Nat. Methods 14, 687–690. 10.1038/nmeth.4324. [PubMed: 28581496]
60. Subramanian A, Tamayo P, Mootha VK, Mukherjee S, Ebert BL, Gillette MA, Paulovich A, Pomeroy SL, Golub TR, Lander ES, and Mesirov JP (2005). Gene set enrichment analysis: a knowledge-based approach for interpreting genome-wide expression profiles. Proc. Natl. Acad. Sci. USA 102, 15545–15550. 10.1073/pnas.0506580102. [PubMed: 16199517]
61. Holdorf AD, Higgins DP, Hart AC, Boag PR, Pazour GJ, Walhout AJM, and Walker AK (2020). WormCat: An Online Tool for Annotation and Visualization of Caenorhabditis elegans Genome-Scale Data. Genetics 214, 279–294. 10.1534/genetics.119.302919. [PubMed: 31810987]
62. Higgins DP, Weisman CM, Lui DS, D'Agostino FA, and Walker AK (2022). Defining characteristics and conservation of poorly annotated genes in Caenorhabditis elegans using WormCat 2.0. Genetics 221, iyac085. 10.1093/genetics/iyac085. [PubMed: 35587742]
63. Danecek P, Bonfield JK, Liddle J, Marshall J, Ohan V, Pollard MO, Whitwham A, Keane T, McCarthy SA, Davies RM, and Li H (2021). Twelve years of SAMtools and BCFtools. GigaScience 10, giab008. 10.1093/gigascience/giab008. [PubMed: 33590861]
64. Quinlan AR, and Hall IM (2010). BEDTools: a flexible suite of utilities for comparing genomic features. Bioinformatics 26, 841–842. 10.1093/bioinformatics/btq033. [PubMed: 20110278]
65. Cingolani P. (2022). Variant Annotation and Functional Prediction: SnpEff. Methods Mol. Biol 2493, 289–314. 10.1007/978-1-0716-2293-3_19. [PubMed: 35751823]
66. Cingolani P, Platts A, Wang LL, Coon M, Nguyen T, Wang L, Land SJ, Lu X, and Ruden DM (2012). A program for annotating and predicting the effects of single nucleotide polymorphisms, SnpEff: SNPs in the genome of Drosophila melanogaster strain w1118; iso-2; iso-3. Fly (Austin) 6, 80–92. 10.4161/fly.19695. [PubMed: 22728672]
67. Ghanta KS, Ishidate T, and Mello CC (2021). Microinjection for precision genome editing in Caenorhabditis elegans. STAR Protoc. 2, 100748. 10.1016/j.xpro.2021.100748. [PubMed: 34505086]
68. Timmons L, Court DL, and Fire A (2001). Ingestion of bacterially expressed dsRNAs can produce specific and potent genetic interference in Caenorhabditis elegans. Gene 263, 103–112. 10.1016/s0378-1119(00)00579-5. [PubMed: 11223248]
69. Conte D Jr., MacNeil LT, Walhout AJM, and Mello CC (2015). RNA Interference in Caenorhabditis elegans. Curr. Protoc. Mol. Biol 109, 26.3.1–26.3.30. 10.1002/0471142727.mb2603s109.
70. Peterson ND, Tse SY, Huang QJ, Wani KA, Schiffer CA, and Pukkila-Worley R (2023). Non-canonical pattern recognition of a pathogen-derived metabolite by a nuclear hormone receptor identifies virulent bacteria in C. elegans. Immunity 56, 768–782.e9. 10.1016/j.immuni.2023.01.027. [PubMed: 36804958]
71. Pfaffl MW (2001). A new mathematical model for relative quantification in real-time RT-PCR. Nucleic Acids Res. 29, e45. [PubMed: 11328886]
72. Tan MW, Mahajan-Miklos S, and Ausubel FM (1999). Killing of *Caenorhabditis elegans* by *Pseudomonas aeruginosa* used to model mammalian bacterial pathogenesis. Proc. Natl. Acad. Sci. USA 96, 715–720. [PubMed: 9892699]

Highlights

- A forward genetic screen uncovered ROTR-1, a suppressor of TIR-1 multimerization
- ROTR-1 maintains lysosome-related organelles (LROs), which express TIR-1
- LRO integrity, ensured by ROTR-1, prevents aberrant TIR-1 aggregation and activation
- Suppression of TIR-1 aggregation restrains toxic propagation of p38 innate immunity

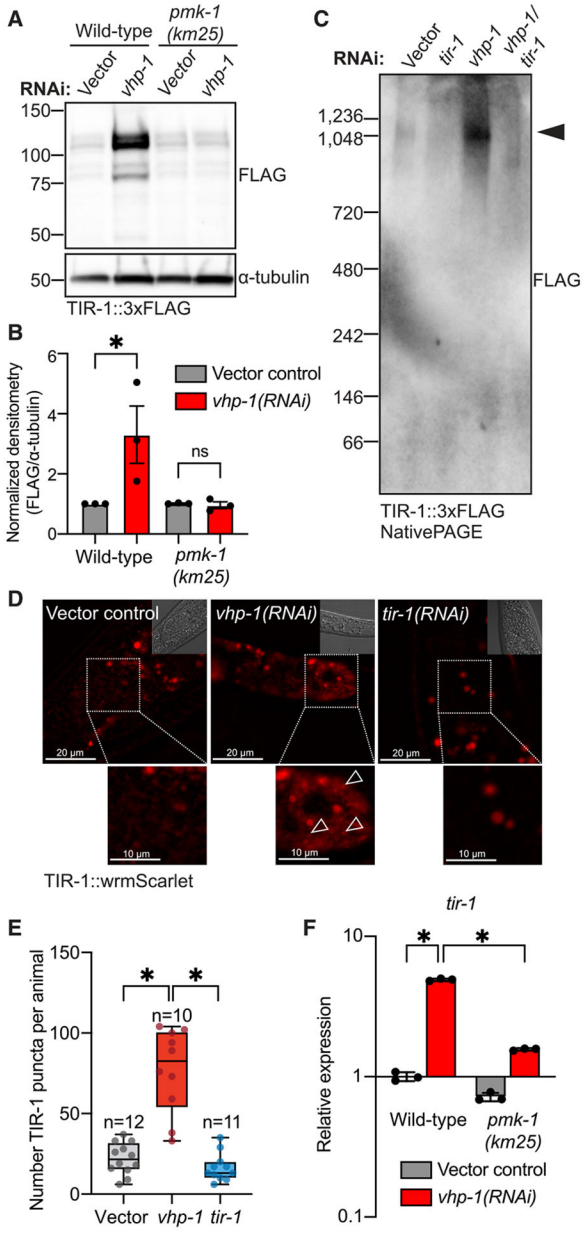

Figure 1. Positive feedback activation of the p38 PMK-1 pathway potentiates innate immune defenses by promoting TIR-1 multimerization

(A) Representative immunoblot using an anti-FLAG antibody on whole-cell lysates of wild-type and *pmk-1(km25)* mutants in the TIR-1::3xFLAG background treated with vector control or *vhp-1(RNAi)*.

(B) Densitometric quantification of (A). Error bars represent SEM ($n = 3$). *$p < 0.05$ (two-way ANOVA with Šídák's multiple comparisons test).

(C) Blue native PAGE immunoblot on *C. elegans* TIR-1::3xFLAG animals treated with vector control, *tir-1(RNAi), vhp-1(RNAi)*, or *vhp-1/tir-1* double RNAi. Immunoblot was probed using the anti-FLAG antibody. Arrowhead indicates TIR-1 multimer. Immunoblot is representative of two independent experiments.

(D) Images of *C. elegans* TIR-1::wrmScarlet animals treated with vector control, *vhp-1(RNAi)*, or *tir-1(RNAi)*. Insets represent corresponding differential interference contrast (DIC) images. Dotted boxes indicate higher magnifications. Open arrowheads indicate TIR-1 puncta.

(E) Quantification of the number of TIR-1::wrmScarlet puncta in (D).[12] Box and whisker plots represent the median with minimum, second quartile, third quartile, and maximum indicated for each condition. $*p < 0.05$ (one-way ANOVA with Tukey's multiple comparisons test). $n = 10–12$ animals per condition and is representative of two independent experiments.

(F) RT-qPCR analysis of *tir-1* transcription in wild-type and *pmk-1(km25)* mutant animals treated with vector control or *vhp-1(RNAi)*. Error bars represent SD ($n = 3$). $*p < 0.05$ (two-way ANOVA with Tukey's multiple comparisons test). Source data for this figure are in Table S3.

See also Figure S1.

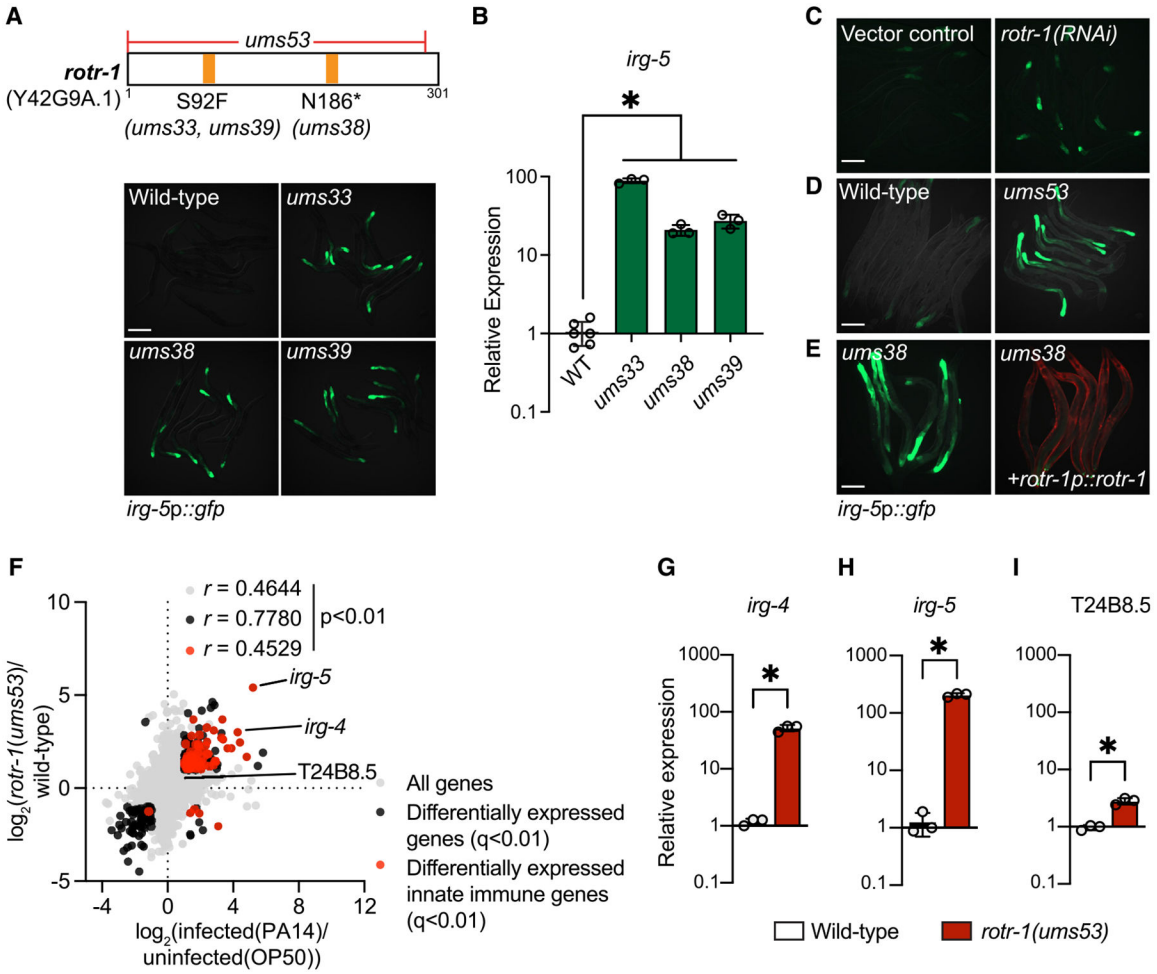

Figure 2. A forward genetic screen identifies *rotr-1*, a suppressor of immune gene transcription

(A) Representative images of forward genetic mutants *ums33, ums38*, and *ums39* in the *irg-5*p::*gfp* reporter background. Specific mutations of each allele are indicated in the schematic of the *rotr-1* protein sequence above the images.

(B) RT-qPCR analysis of *irg-5* transcription in the forward genetic mutants in (A). Data are the mean of replicates with error bars giving SD. **p* < 0.05 (one-way ANOVA with Dunnett's multiple comparisons test).

(C) Representative images of *irg-5*p::*gfp* animals treated with *rotr-1(RNAi)*.

(D) Representative images of wild-type and CRISPR-Cas9-generated *rotr-1(ums53)* clean deletion mutant in the *irg-5*p::*gfp* reporter background.

(E) Representative images of *rotr-1(ums38)*, a mutant isolated from the forward genetic screen, that was rescued with a transgene expressing *rotr-1* under its own promoter, as indicated. Red indicates *myo-3*p::*mCherry* expression and is the co-injection marker.

(F) Data from mRNA-seq experiments comparing genes differentially regulated in uninfected *rotr-1(ums53)* mutants versus wild-type animals or uninfected wild-type animals versus *P. aeruginosa*-infected wild-type animals. All genes are shown in gray. Genes that are differentially expressed in both datasets are shown in black (fold change > 2, q < 0.01). Innate immune genes are shown in red. The locations of *irg-4, irg-5*, and T24B8.5 are

indicated. Note that T24B8.5 is only significantly differentiated in infected animals. See also Table S1.

(G–I) RT-qPCR analyses comparing the transcription of *irg-4* (G), *irg-5* (H), and T24B8.5 (I) in wild-type and *rotr-1(ums53)* null mutants. Data are the mean of replicates with error bars giving SD. *$p < 0.05$ (unpaired t test) ($n = 3$). Source data for this figure are in Table S3. Scale bars represent 200 μm.

See also Figure S2.

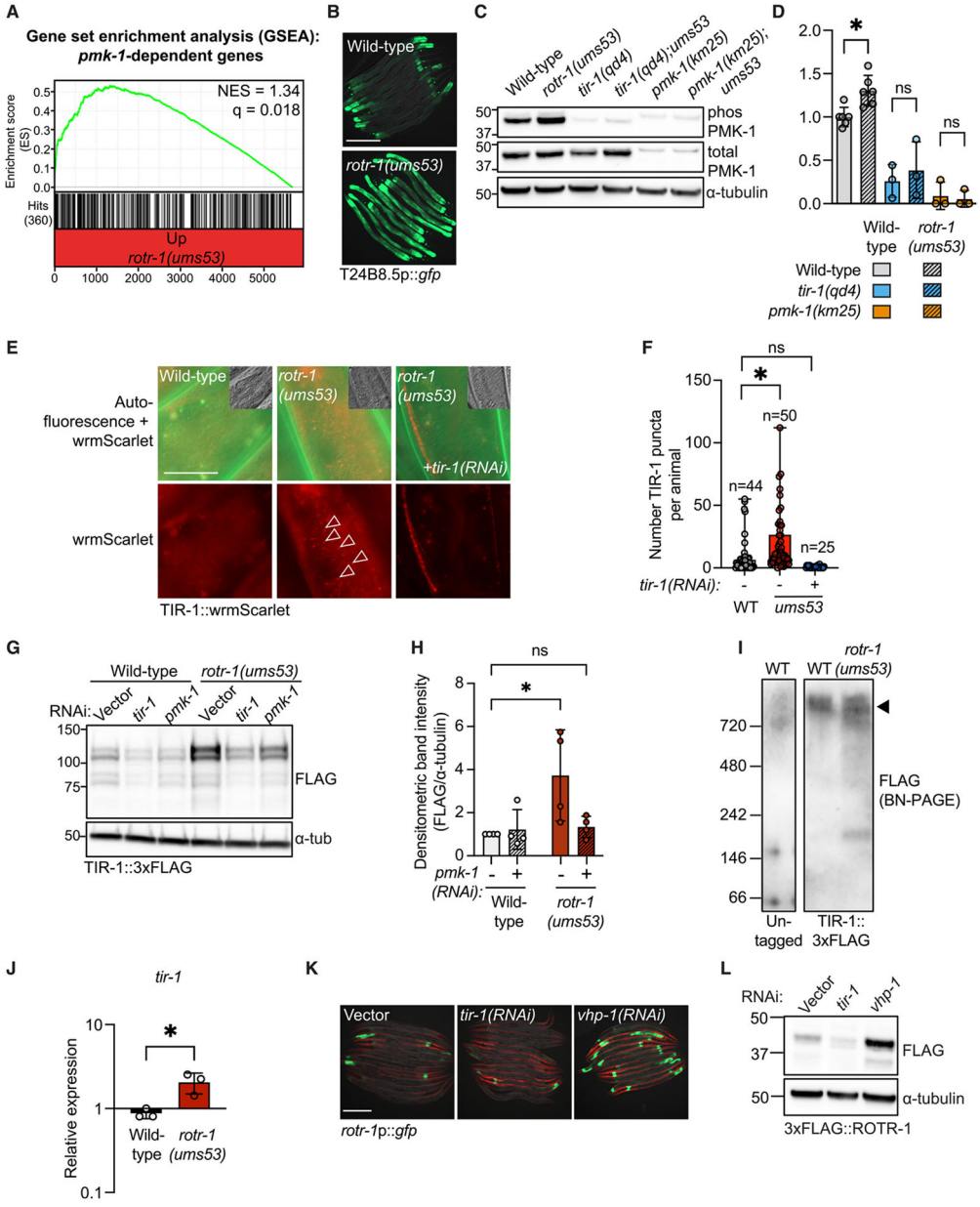

Figure 3. ROTR-1 suppresses positive feedback activation of p38 PMK-1 innate immunity

(A) Gene set enrichment analysis of p38 PMK-1 targets in the *rotr-1(ums53)* mRNA-seq experiment. Each differentially upregulated gene in *rotr-1(ums53)* mutants was assigned a π value[25] and ranked from highest to lowest. The normalized enrichment score (NES) and q value are indicated. p38 PMK-1 targets identified are indicated by hit number and black lines below the graph.

(B) Representative images of wild-type and *rotr-1(ums53)* null mutants in the T24B8.5p::*gfp* transcriptional reporter animals.

(C) Representative immunoblot of whole-cell lysates from indicated genotypes that were probed for anti-phosphorylated PMK-1, anti-total PMK-1, and anti-α-tubulin.

(D) Densitometric quantification of (C). Data are mean of replicates with error bars representing SEM (n = 3–6). *p < 0.05 (two-way ANOVA with Šídák's multiple comparisons test).

(E) Images of wild-type or *rotr-1(ums53)* mutants expressing TIR-1::wrmScarlet. Insets represent corresponding DIC images. Arrowheads indicate TIR-1::wrmScarlet puncta. Scale bar represents 200 μm.

(F) Quantification of TIR-1::wrmScarlet puncta in (E).[12] Box and whisker plots represent the median with minimum, second quartile, third quartile, and maximum indicated for each condition. *p < 0.05 (one-way ANOVA with Dunnett's multiple comparisons test). ns, not significant. The number of animals analyzed is indicated above each bar. Representative of two independent experiments.

(G) Representative immunoblot of whole-cell lysates from wild-type and *rotr-1(ums53)* in the TIR-1::3xFLAG background treated with indicated RNAi and probed with anti-FLAG or anti-α-tubulin. Immunoblot is representative of 4 independent replicates.

(H) Densitometric quantification of vector control and *pmk-1(RNAi)* conditions in (G). Data are the mean of replicates with error bars giving SEM. *p < 0.05 (two-way ANOVA with Šídák's multiple comparisons test).

(I) Blue native PAGE immunoblot on wild-type and *rotr-1(ums53)* mutants in the TIR-1::3xFLAG background. Multimers are indicated by the arrowhead. Immunoblot of untagged animals is shown on the left. Immunoblot was probed using the anti-FLAG antibody. Immunoblot is representative of two independent experiments.

(J) RT-qPCR analysis of *tir-1* transcription in wild-type and *rotr-1(ums53)* mutants. Error bars represent SEM (n = 3). *p < 0.05 (unpaired t test).

(K) Representative images of animals expressing a *gfp* transcriptional fusion under the control of the *rotr-1* promoter (*rotr-1p::gfp*) treated with vector control, *tir-1(RNAi)*, or *vhp-1(RNAi)*.

(L) Immunoblot of whole-cell lysates from 3xFLAG::ROTR-1 animals treated with vector control, *tir-1(RNAi)*, or *vhp-1(RNAi)*. Scale bars represent 200 μm. Source data for this figure are in Table S3.

See also Figure S3.

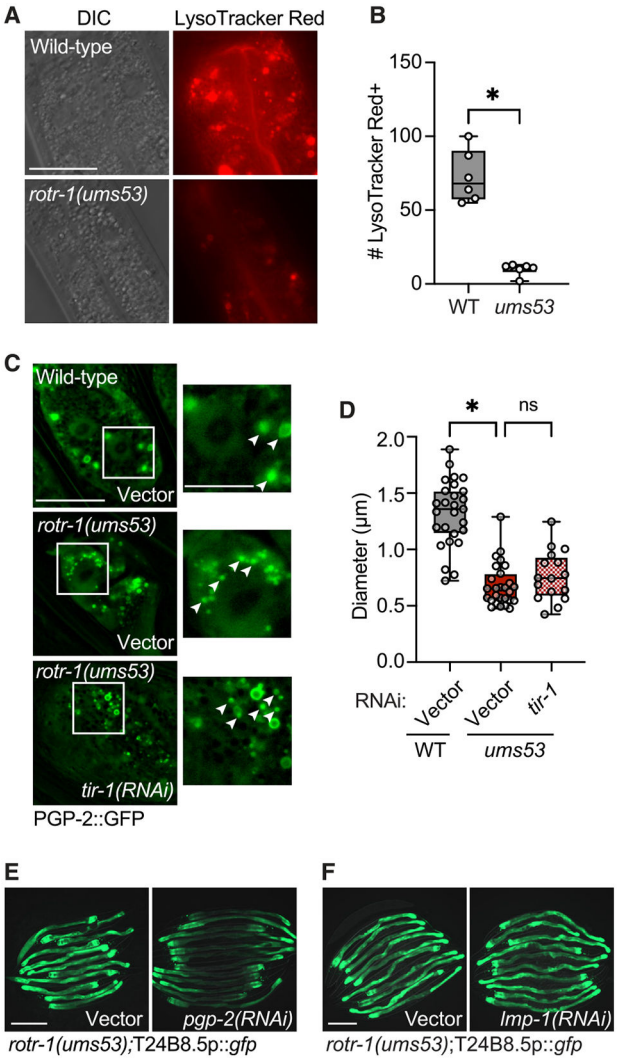

Figure 4. ROTR-1 supports the integrity of lysosome-related organelles, which restrains positive feedback activation of p38 PMK-1 innate immunity

(A) Representative images of wild-type and *rotr-1(ums53)* mutants stained with LysoTracker red (1 µM). DIC images are shown on the left. Scale bar represent 20 µm.

(B) Quantification of the number of LysoTracker red(+) vesicles in wild-type and *rotr-1(ums53)* mutants using Fiji. Each data point represents one animal ($n = 6$). Box and whisker plots represent the median with minimum, second quartile, third quartile, and maximum indicated for each condition. *$p < 0.05$ (unpaired t test).

(C) Images of wild-type and *rotr-1(ums53)* mutants expressing PGP-2::GFP (lysosome-related organelles) treated with vector control or *tir-1(RNAi)*. Boxes indicate areas shown at higher magnification to the right. Scale bar represents 20 µm for lower magnification and 10 µm for higher magnification. Arrowheads indicate individual lysosome-related organelles.

(D) Quantification of the diameter of PGP-2::GFP(+) vesicles in indicated conditions. Each data point represents one animal. Box and whisker plots represent the median with minimum, second quartile, third quartile, and maximum indicated for each condition. *$p <$

0.05; ns, not significant (one-way ANOVA with Dunnett's multiple comparisons test). Data are representative of two independent experiments.

(E and F) Representative images of *rotr-1(ums53)* mutants in the T24B8.5p::gfp background treated with vector control or *pgp-2(RNAi)* (E) or *lmp-1(RNAi)* (F). Scale bar represents 200 μm. See Table S3.

See also Figure S4.

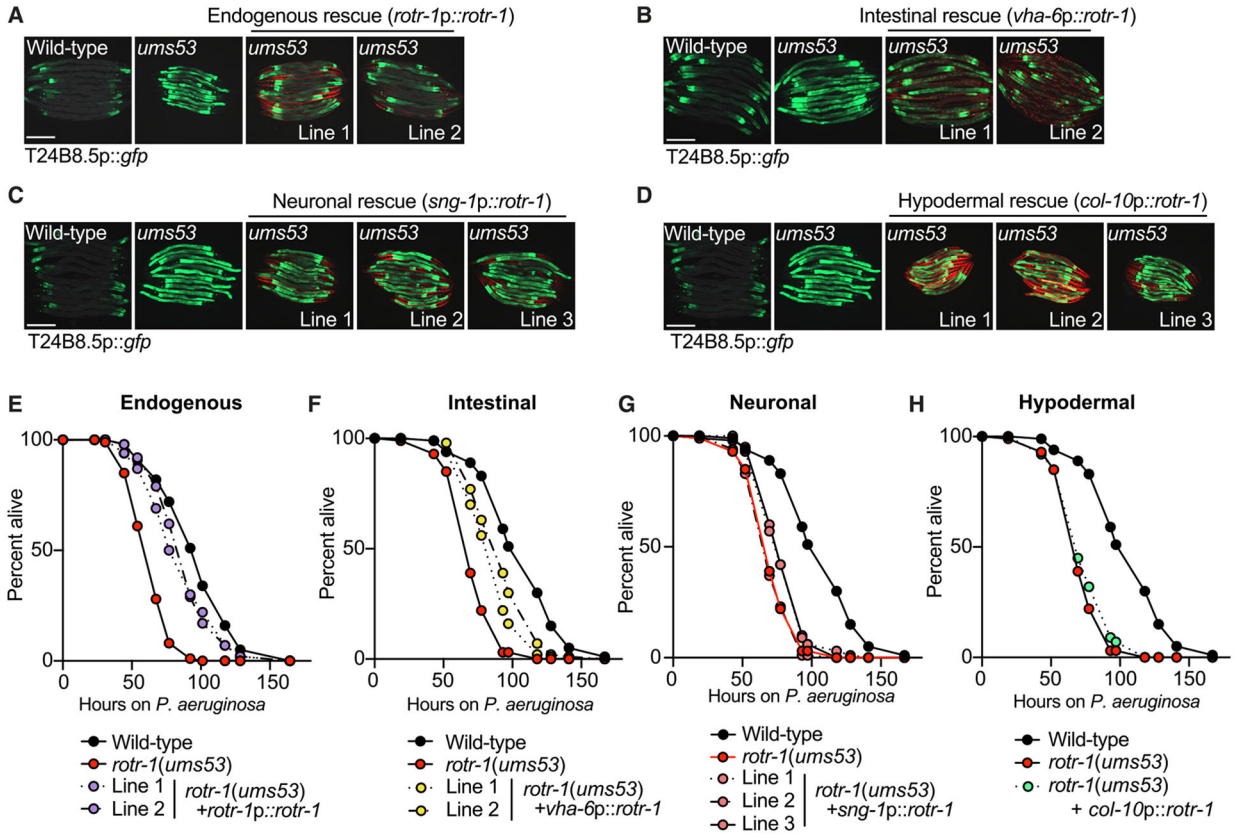

Figure 5. ROTR-1 functions in the *C. elegans* intestine

(A–D) Images of wild-type and *rotr-1(ums53)* mutants expressing transgenes of *rotr-1* under the indicated promoters for endogenous *rotr-1* expression (*rotr-1*p::*rotr-1*) (A), intestinal *rotr-1* expression (*vha-6*p::*rotr-1*) (B), neuronal *rotr-1* expression (*sng-1*p::*rotr-1*) (C), and hypodermal expression (*col-10*p::*rotr-1*) (D). Tissue-specific expression of *rotr-1* in these strains was confirmed using a construct that contains a split-leader mCherry sequence for *his-58*, which labeled the nuclei of tissues with *rotr-1* expression in red.

(E–H) Representative *P. aeruginosa* pathogenesis assays for strains indicated in (A)–(D). Note that only one hypodermal *rotr-1* rescue line is represented due to the toxicity of hypodermal expression of *rotr-1*. The difference between each rescue line and the *rotr-1(ums53)* mutant is significant in (E) and (F) ($p < 0.05$, log-rank test). Scale bars represent 200 μm. Sample size (*n*), mean lifespans, and statistics for all replicates are in Table S2A.

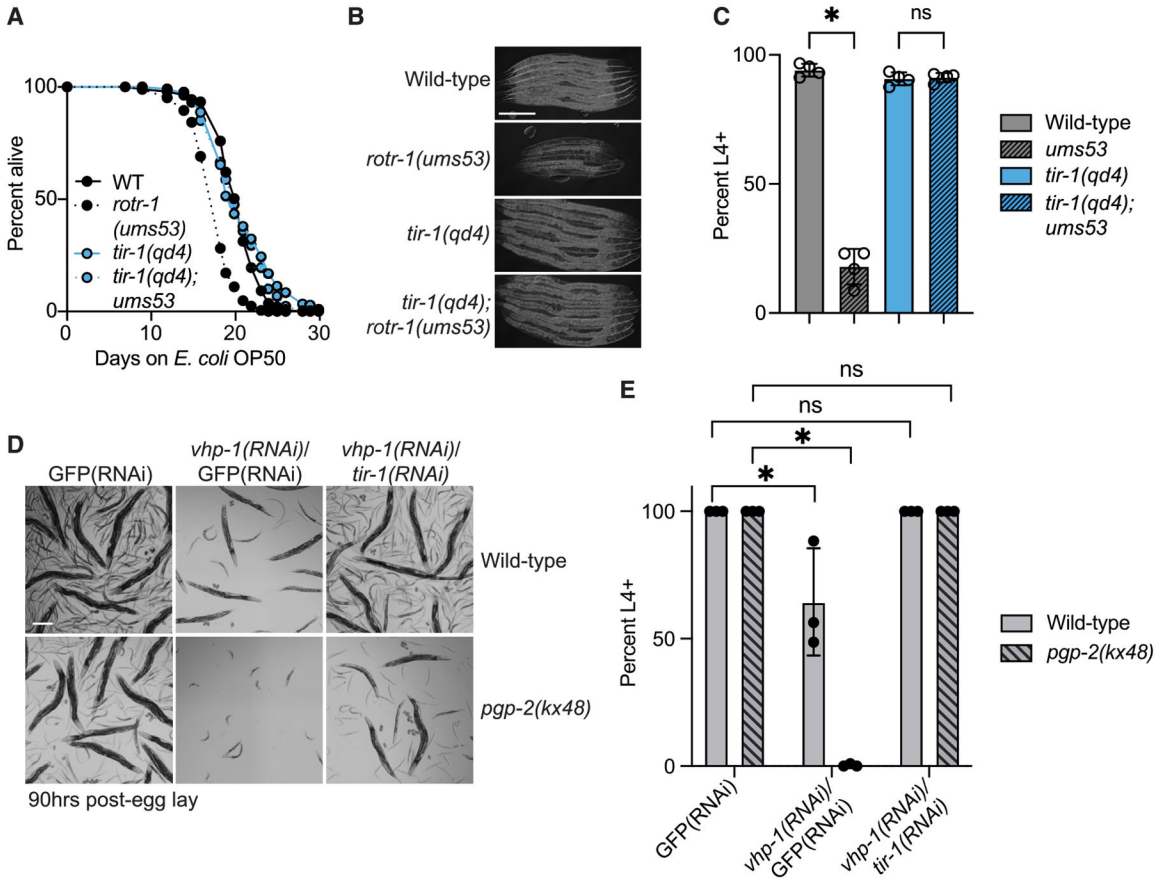

Figure 6. Lysosome-related organelle integrity, ensured by ROTR-1, restrains toxic propagation of p38 PMK-1 innate immunity

(A) Representative lifespan assay of wild-type, *rotr-1(ums53), tir-1(qd4),* and *tir-1(qd4);rotr-1(ums53)* mutants.

(B and D) Images of indicated *C. elegans* genotypes in a developmental assay. Scale bar represents 200 μm.

(C and E) Development assay of indicated *C. elegans* genotypes quantifying the percentage of animals older than the larval L4 stage. Data are the mean of replicates with error bars giving SEM. *$p < 0.05$; ns, not significant (one-way ANOVA with Dunnett's multiple comparisons test). Source data for this figure is in Table S3. Sample size (n), mean lifespans, and statistics for all replicates are in Tables S2B and S2C.

KEY RESOURCES TABLE

REAGENT or RESOURCE	SOURCE	IDENTIFIER
Antibodies		
Anti-FLAG M2, Mouse, Monoclonal, Unconjugated	Sigma-Aldrich	Cat# F1804; RRID:AB_262044
Anti-alpha-Tubulin, Mouse, Monoclonal, Unconjugated	Sigma-Aldrich	Cat# T5168; RRID:AB_477579
Anti-phospho-p38 MAPK (Thr180/Tyr182), Rabbit	Cell Signaling Technology	Cat # 9211S; RRID:AB_331641
Anti-HA High Affinity, Rat	Roche	Cat# 11867423001; RRID:AB_390918
Anti-total-p38 MAPK, Rabbit	(Peterson et al.)[24]	N/A
Anti-ROTR-1, Rabbit, sera	This study	N/A
Goat Anti-Rabbit IgG, HRP-linked	Cell Signaling Technology	Cat# 7074; RRID:AB_2099233
Goat Anti-Mouse IgG – H&L, Polyclonal, HRP Conjugated	Abcam	Cat# ab6789; RRID:AB_955439
Goat Anti-Rat IgG H&L, HRP-linked	Abcam	Cat# ab97057; RRID:AB_10680316
Bacterial and virus strains		
Escherichia coli OP50	(Brenner et al.)[51]	WB Cat# WBStrain00041969; RRID:WB-STRAIN: WBStrain00041969
E. coli HT115(DE3)	(Fire et al.)[52]	WB Cat# WBStrain00041080; RRID:WB-STRAIN: WBStrain00041080
Pseudomonas aeruginosa (UCBPP-PA14)	(Rahme et al.)[53]	RRID:WB-STRAIN: WBStrain00041978
Chemicals, peptides, and recombinant proteins		
Ethyl methanesulfonate (EMS)	Sigma-Aldrich	Cat# M0880
5-Fluoro-2′-deoxyuridine (FUDR)	Sigma-Aldrich	Cat# CAF0503
(−) Tetramisole hydrochloride	Sigma-Aldrich	Cat# L9756–10G
Isopropyl-β-D-thiogalactoside (IPTG)	GoldBio	Cat# I2481C200
Trizol	Thermo Fisher Scientific	Cat# 15596018
Proteinase K	New England BioLabs	Cat# P8107S
Ethylenediaminetetraacetic acid (EDTA), 0.5M, pH 8.0	Thermo Fisher Scientific	Cat# 1860851
HALT Protease Inhibitor Cocktail (100X)	Thermo Fisher Scientific	Cat# 78430
Phenol:chloroform:isoamyl alcohol	Thermo Fisher Scientific	Cat# 15593031
SpCas9 Nuclease	IDT	Cat# 1081058
Streptomycin sulfate	Thermo Fisher Scientific	Cat# AC612240500
LysoTracker™ Red DND-99	Invitrogen	Cat# L7528
Bacto-peptone	Thermo Fisher Scientific	Cat# 211677
Fisher agar	Fisher	Cat# BP9744500
Critical commercial assays		
iScript gDNA Clear cDNA Synthesis Kit	Bio-Rad	Cat# 172-5034
DC Protein Assay	Bio-Rad	Cat# 5000111

REAGENT or RESOURCE	SOURCE	IDENTIFIER
iTaq Universal SYBR Green Supermix	Bio-Rad	Cat# 172-5120
SuperSignal West Pico	Thermo Fisher	Cat# 34580
SuperSignal West Femto	Thermo Fisher	Cat# 34094
NativePAGE™ Running Buffer Kit	Invitrogen	Cat# BN2007
Gentra® Puregene® Cell and Tissue Kit	Qiagen	Cat# 158388
RNeasy MinElute Cleanup Kit	Qiagen	Cat# 74204
Deposited data		
Raw and analyzed mRNA-seq data	This study	GEO: GSE256356
Experimental models: Organisms/strains		
C. elegans: Strain: N2 (Bristol)	(Brenner et al.)[51]	WB Cat# WBStrain00000001; RRID:WB-STRAIN: WBStrain00000001
C. elegans: AU78 *agIs219* [T24B8.5p:*gfp*::*unc-54*-3′UTR; *ttx-3*p::*gfp::unc-54*-3′UTR] *III*	(Shivers et al.)[11]	WB Cat# WBStrain00000262
C. elegans: RPW403 *ums63* [TIR-1:wrmScarlet]	(Peterson et al.)[12]	N/A
C. elegans: RPW446 *ums63* [TIR-1:wrmScarlet]; *rotr-1(ums53)*	This study	N/A
C. elegans: RPW386 *ums57* [TIR-1:3xFLAG]; *agIs219*	(Peterson et al.)[12]	N/A
C. elegans: AY101 *acIs101* [pDB09.1(irg-5p::gfp); pRF4(*rol-6(su1006)*]	(Bolz et al.)[44]	N/A
C. elegans: RPW503 *ums57* [TIR-1:3xFLAG]; *pmk-1(km25); agIs219*	This study	N/A
C. elegans: RPW504 *ums57* [TIR-1:3xFLAG]; *kgb-1(km21); agIs219*	This study	N/A
C. elegans: RPW262 *acIs101* [pDB09.1(*irg-5p::gfp*); pRF4(*rol-6(su1006)*]; *rotr-1(ums33)*	This study	N/A
C. elegans: RPW267 *acIs101* [pDB09.1(*irg-5p::gfp*); pRF4(*rol-6(su1006)*]; *rotr-1(ums38)*	This study	N/A
C. elegans: RPW272 *acIs101* [pDB09.1(*irg-5p::gfp*); pRF4(*rol-6(su1006)*]; *rotr-1(ums39)*	This study	N/A
C. elegans: RPW366 *acIs101* [pDB09.1(*irg-5p::gfp*); pRF4(*rol-6(su1006)*]; *rotr-1(ums53)*	This study	N/A
C. elegans: RPW356 *agIs219* [T24B8.5p:*gfp::unc54*-3′UTR; *ttx-3p::gfp::unc-54*-3′UTR] III; *rotr-1(ums53)*	This study	N/A
C. elegans: RPW384 *agIs219; rotr-1(ums53); umsEx78 [rotr-1p::rotr-1; myo-3p::mCherry]*_Line 1	This study	N/A
C. elegans: RPW385 *agIs219; rotr-1(ums53); umsEx79* [*rotr-1*p::rotr-1; *myo-3*p::*mCherry*]_Line 2	This study	N/A
C. elegans: RPW415 *agIs219; rotr-1 (ums53); umsEx83* [*vha-6p::rotr-1*::SL2:mCherry; *myo-3*p::mCherry]_Line 1	This study	N/A
C. elegans: RPW416 *agIs219; rotr-1* (*ums53*); *umsEx84* [*vha-6*p::*rotr-1* ::SL2:mCherry; *myo*-3p::mCherry]_Line 2	This study	N/A
C. elegans: RPW417 *agIs219; rotr-1(ums53); umsEx85* [*sng-1*p::*rotr-1*::SL2:mCherry; *myo-3*p::mCherry]_Line 1	This study	N/A
C. elegans: RPW418 *agIs219; rotr-1 (ums53); umsEx86* [*sng-1p::rotr-1*::SL2:mCherry; *myo-3*p::mCherry]_Line 2	This study	N/A
C. elegans: RPW419 *agIs219; rotr-1 (ums53); umsEx87* [*sng-1*p::*rotr-1*::SL2:mCherry; *myo-3*p::mCherry]_Line 3	This study	N/A
C. elegans: RPW442 *agIs219; rotr-1(ums53); umsEx95* [*col-10*p::*rotr-1*::SL2:mCherry; *myo-3*p::mCherry]_Line 1	This study	N/A

REAGENT or RESOURCE	SOURCE	IDENTIFIER
C. elegans: RPW443 *agIs219; rotr-1(ums53); umsEx96* [*col-10*p::*rotr-1*::SL2:mCherry; *myo-3*p::mCherry]_Line 2	This study	N/A
C. elegans: RPW444 *agIs219; rotr-1(ums53); umsEx97* [*col-10*p::*rotr-1*::SL2:mCherry; *myo-3*p::mCherry]_Line 3	This study	N/A
C. elegans: RPW398 *umsEx132* [*rotr-1*p::*gfp*; *myo-3*p::mCherry]	This study	N/A
C. elegans: RPW420 *rotr-1(ums53); ums57* [TIR-1:3xFLAG]; *agIs219*	This study	N/A
C. elegans: RPW447 *ums81* [ROTR-1:3xHA]; *agIs219*	This study	N/A
C. elegans: RPW471 *ums75* [3xFLAG::ROTR-1]; *agIs219*	This study	N/A
C. elegans: MGH41 *alxIs1* [*vha*-6p::PGP-2:GFP; pRF4(*rol-6(su1006)*)]	Soukas lab, unpublished	N/A
C. elegans: RT258 *pwIs50* [LMP-1:GFP + Cbr-unc-119(+)]	(Treusch et al.)[54]	N/A
C. elegans: RPW527 *alxIs1* [*vha-6*p::PGP-2:GFP; pRF4(*rol-6(su1006)*)];*tir-1(ums63); rotr-1(ums53)*	This study	N/A
C. elegans: RPW526 *pwIs50* [LMP-1:GFP + Cbr-unc-119(+)];*tir-1(ums63); rotr-1(ums53)*	This study	N/A
Oligonucleotides		
See Table S4	This study	N/A
Software and algorithms		
Fiji/ImageJ	(Schindelin et al.)[55]	RRID:SCR_002285
OASIS 2	(Han et al.)[56]	RRID:SCR_014450
Zen (version 2.5)	Zeiss	RRID:SCR_013672
LasX (version 1.4.5)	Leica	RRID:SCR_013673
CHOPCHOP (version 3)	(Labun et al.)[57]	RRID:SCR_015723
R Console (version 3.5)	The R Foundation	RRID:SCR_000432
FastQC (version 0.11.5)	https://www.bioinformatics.babraham.ac.uk/projects/fastqc/	RRID:SCR_014583
Kallisto (version 0.45.0)	(Bray et al.)[58]	RRID:SCR_016582
Sleuth (version 0.30.0)	(Pimental et al.)[59]	RRID:SCR_002555
GSEA (version 4.1.0)	(Subramanian et al.)[60]	RRID:SCR_003199
WormCat 2.0	(Holdorf et al. and Higgins et al.)[61,62]	N/A
BCFtools (version 1.10.2)	(Danecek et al.)[63]	RRID:SCR_005227
BEDtools (version 2.29.2)	(Quinlan et al.)[64]	RRID:SCR_006646
SnpEff (version 5.2)	(Cingolani and Cingolani et al.)[65,66]	RRID:SCR_005191
GraphPad Prism 10	https://www.graphpad.com/scientific-software/prism/	RRID: SCR_002798
Other		
Leica THUNDER DMi8	Leica	RRID:SCR_023794
Zeiss Axio Imager 506 mono camera	Zeiss	RRID:SCR_024706